
University of Crete
Department of Physics

MSc Diploma Thesis

# Using optical aberrations as wavefront modulators

**Panagiotis Zavitsanos**

Supervisor: Dimitris Papazoglou, Associate Professor,
Department of Materials Science and Technology,
University of Crete

Comittee members:

Kostantinos Makris, Assistant Professor,
Physics Department, University of Crete

Peter Rakitzis, Professor
Physics Department, University of Crete

Heraklion, June 2022

**Abstract**

In this thesis we have studied imaging systems that use optical aberrations to perform as continuous phase modulation devices.

Compared to Diffracting Optical Elements (DOEs) and Spatial Light Modulators (SLMs) these devices are in principle scalable both in respect of input power and bandwidth, making it possible to be used in any part of the electromagnetic spectrum. Furthermore, we evaluate, both analytical and numerical, design strategies that allow the realization of such tunable, continuous phase modulation devices.

**Περίληψη**

Σε αυτή την εργασία εξετάσαμε συστήματα απεικόνισης τα οποία αξιοποιούν τα οπτικά σφάλματα απεικόνισης έτσι ώστε να λειτουργούν ως συσκευές συνεχούς διαμόρφωσης μετώπου κύματος.

Σε σύγκριση με τα περιθλαστικά οπτικά στοιχεία (DOEs) ή τους χωρικούς διαμορφωτές φωτός (SLMs), οι συσκευές αυτές είναι επεκτάσιμες όσον αφορά τα όρια λειτουργίας τους σε σχέση με το φασματικό εύρος αλλά και την οπτική ισχύ που μπορούν να διαχειριστούν, καθιστώντας έτσι δυνατή την λειτουργία τους σε οποιαδήποτε κομμάτι του ηλεκτρομαγνητικού φάσματος. Επιπλέον, αξιολογήσαμε, τόσο με αναλυτικές όσο και με αριθμητικές μεθόδους, στρατηγικές οπτικής σχεδίασης που επιτρέπουν την υλοποίηση τέτοιων συσκευών.

# Contents

# Introduction

Optical aberrations can be thought of as an extension of the paraxial theory of optics. Within the validity of paraxial optics one can robustly define the relation between the object space and the image space. Rays coming from an object point collapse into a single point in the image space i.e the image point. Since the paraxial theory is itself based on some key assumptions, mentioned in chapter 3, it is only natural that optical systems that do not meet those assumptions can not accurately be described by the theory. In practice all optical systems and configurations only partially meet the criteria of the paraxial theory. As a result optical aberrations are always present in an optical system degrading the image quality. Optical aberrations can be monochromatic or chromatic. The first type exists even for quasimonochromatic light, deteriorating and deforming the image. The latter results from the fact that the refractive index is a function of frequency.

In the context of geometrical optics, light propagates along straight lines called rays. A family of rays forms a ray bundle also known as a pencil of rays. The surface orthogonal to the pencil of rays is called the wavefront. Within the paraxial theory a sharp focus corresponds to a spherical wavefront where the focus lies in the center of the sphere. In real systems the lack of homocentricity of the image forming pencil of rays results to the departure of the wavefront from the spherical form. The difference between the real and the ideal (spherical) wavefront is quantified by optical aberrations. On that account we can envisage optical aberrations as smooth perturbations on the spherical wavefront. It is a well known fact in optical design that monochromatic aberrations result from the surface type of the optical elements as well as their positioning in three dimensional space. Consequently a small change of those parameters will introduce some perturbation on the corresponding wavefront and provides a way of wavefront modulation. Optical systems that modulate the wavefront in such a way have been implemented successfully[7],[8] by isolating specific aberration terms as well as reconstructing polynomial space phase distributions.

In this project we investigate an optical system consisting of mainly two reflective cylindrical surfaces in a beam expander configuration [7]. By changing the orientation as well as the distance between the two mirrors we introduce aberrations to the wavefront. At first with the use of a raytracing software we check its ability to isolate specific aberration terms. Moreover by making proper adjustments to the set up we show that any continuous spacial phase distribution can be generated by combining different aberration terms together. Its bandwidth of operation is also considered since all elements are reflective leading to ultra-broadband phase modulation. Furthermore we exploit its use as a continuous phase mask by varying its parameters in order to achieve infrared wavefront modulation as well as experimenting with stacking configurations. At last, with the use of our own raytracing program that can also handle symbolic calculations we derive an analytic expression for the total optical path length a ray traverses as a function of the input variable ( that defines the starting position of the rays) and system parameters.At last by establishing a linear relation between the input and output variables (screen coordinates) we calculate the total optical path as a function of system parameters and output coordinates in the form of a series approximation for a $2D$ analogue of our system.

# 1 From Maxwell equations to Geometrical Optics

## 1.1 Maxwell's equations

Geometrical optics are defined as the limiting case of wave optics for very small wavelengths $\lambda \to 0$. It is well known that such an approximation holds well for the case of visible light, X-rays and gamma radiation since the field is characterized by very rapid oscillations and the wavelength is negligible $\lambda < 10^{-6}$ m. In such cases the optical laws may be formulated in the language of geometry, and directly be used in order to solve problems provided that the size of optical elements and especially stops are not of the order of the wavelength. Within the limits of such an approximation the energy may be regarded as being transported along curves (light rays).

The basic equations of geometrical optics are derived directly from Maxwell's equations for the case of linear isotropic materials. Additionally the electric charge density $\rho$ as well as the current density $\mathbf{j}$ are assumed to be zero. The four Maxwell equations become :

$$\nabla \times \mathbf{E}(\mathbf{r},t) = -\frac{\partial \mathbf{B}(\mathbf{r},t)}{\partial t} \tag{1.1}$$

$$\nabla \times \mathbf{H}(\mathbf{r},t) = \frac{\partial \mathbf{D}(\mathbf{r},t)}{\partial t} \tag{1.2}$$

$$\nabla \cdot \mathbf{B}(\mathbf{r},t) = 0 \tag{1.3}$$

$$\nabla \cdot \mathbf{D}(\mathbf{r},t) = 0 \tag{1.4}$$

where $\mathbf{E}, \mathbf{H}, \mathbf{D}, \mathbf{B}, \mathbf{j}$ are the electric vector, magnetic vector, electric displacement, magnetic induction. In the case of linear and isotropic materials they are linked :

$$\mathbf{D}(\mathbf{r},t) = \epsilon_0 \epsilon(\mathbf{r}) \mathbf{E}(\mathbf{r},t) \tag{1.5}$$

$$\mathbf{B}(\mathbf{r},t) = \mu_0 \mu(\mathbf{r}) \mathbf{H}(\mathbf{r},t) \tag{1.6}$$

$$\tag{1.7}$$

Here $\epsilon$ is the dielectic function, $\mu$ is the magnetic permeability. Also the constants $\epsilon_0$ and $\mu_0$ are the dielectric and magnetic permeability constant of the vacuum.

The electric and magnetic field can be in general described using the form [3].

$$\mathbf{E}(\mathbf{r},t) = \mathbf{e}(\mathbf{r}) e^{ik_0 \mathcal{L}(\mathbf{r})} e^{-i\omega t} \tag{1.8}$$

$$\mathbf{H}(\mathbf{r},t) = \mathbf{h}(\mathbf{r}) e^{ik_0 \mathcal{L}(\mathbf{r})} e^{-i\omega t} \tag{1.9}$$

where $\mathcal{L}$ is the optical path and is a real scalar that depends on position , $\omega$ is the angular frequency and $k_0 = 2\pi/\lambda$ is the wavenumber. The polarization vectors $\mathbf{e}, \mathbf{h}$ are in general complex valued and depend on position. Substituting the above into Maxwell's equations we get :

$$\nabla \times [\mathbf{e}(\mathbf{r}) e^{ik_0 L(\mathbf{r})}] = i\omega \mu(\mathbf{r}) \mu_0 \mathbf{h}(\mathbf{r}) e^{ik_0 L(\mathbf{r})} \tag{1.10}$$

$$\nabla \times [\mathbf{h}(\mathbf{r}) e^{ik_0 L(\mathbf{r})}] = [-i\omega \epsilon(\mathbf{r}) \epsilon_0 + \sigma(\mathbf{r})] e^{ik_0 L(\mathbf{r})} \tag{1.11}$$

$$\nabla \cdot [\mu(\mathbf{r}) \mu_0 \mathbf{h}(\mathbf{r}) e^{ik_0 L(\mathbf{r})}] = 0 \tag{1.12}$$

$$\nabla \cdot [\epsilon(\mathbf{r}) \epsilon_0 \mathbf{e}(\mathbf{r}) e^{ik_0 L(\mathbf{r})}] = 0 \tag{1.13}$$

Here relations (2.10) and (2.12) again with (2.11) and (2.13) are not independent of each other recalling that for an arbitrary vector function $\mathbf{f}$ the identity $\nabla \cdot (\nabla \times \mathbf{f}) = 0$ holds. So if one of them is satisfied so is the other. Carrying out the necessary algebraic manipulations $(2.10), (2.11)$ become :

$$\nabla L(\mathbf{r}) \times \mathbf{e}(\mathbf{r}) - c\mu(\mathbf{r})\mu_0 \mathbf{h}(\mathbf{r}) = \frac{i}{k_0} \nabla \times \mathbf{e}(\mathbf{r}) \tag{1.14}$$

$$\nabla L(\mathbf{r}) \times \mathbf{h}(\mathbf{r}) + c\epsilon(\mathbf{r})\epsilon_0 \mathbf{e}(\mathbf{r}) = \frac{i}{k_0} \nabla \times \mathbf{h}(\mathbf{r}) \tag{1.15}$$

*Geometrical optics approximation:*
We can see that when $\lambda \to 0 \Rightarrow k_0 \to \infty$ the right hand side of both equations becomes zero leading to

$$\nabla L(\mathbf{r}) \times \mathbf{e}(\mathbf{r}) - c\mu(\mathbf{r})\mu_0 \mathbf{h}(\mathbf{r}) = 0 \tag{1.16}$$

$$\nabla L(\mathbf{r}) \times \mathbf{h}(\mathbf{r}) + c\epsilon(\mathbf{r})\epsilon_0 \mathbf{e}(\mathbf{r}) = 0 \tag{1.17}$$

Solving (2.16) for $\mathbf{h}(\mathbf{r})$ and substituting in (2.17) we get

$$[\nabla L(\mathbf{r}) \cdot \mathbf{e}(\mathbf{r})] \nabla L(\mathbf{r}) - [\nabla L(\mathbf{r})]^2 + n^2(\mathbf{r}) \mathbf{e}(\mathbf{r}) = 0 \tag{1.18}$$

From (2.16) and (2.17) we can clearly see that on one hand $\mathbf{h}$ is perpendicular to both $\mathbf{e}$ and $\nabla L$ and on the other that $\mathbf{e}$ is perpendicular to $\mathbf{h}$ as well as $\nabla L$. So in the limiting case where $\lambda \to 0$ $\mathbf{e}$, $\mathbf{h}$ and $\nabla L(\mathbf{r})$ form an orthogonal triad of vectors. On that account the term $\nabla L(\mathbf{r}) \cdot \mathbf{e}$ on (2.18) vanishes and we end up with

$$[\nabla L(\mathbf{r})]^2 = n^2(\mathbf{r}) \tag{1.19}$$

This is known as the eikonal equation of geometrical optics and as we will see it provides a robust basis for the concept of rays.

## 1.2 Ray propagation

It is well known that in isotropic media the direction of propagation $\mathbf{k}$ of an electromagnetic wave coincides with the direction of energy flow, described by the Poynting vector $\mathbf{S}$ . The time averaged Poynting vector for the case of stationary monochromatic waves in the limiting case $\lambda \to 0$ takes the form [3]

$$\langle \mathbf{S} \rangle = \frac{1}{2\mu} \operatorname{Re}(\mathbf{e} \times \mathbf{h}^*) \tag{1.20}$$

Using (2.16) we obtain

$$\langle \mathbf{S} \rangle = \frac{c}{2\mu}[(\mathbf{e} \cdot \mathbf{e}^*)\nabla L - (\mathbf{e} \cdot \nabla L)\mathbf{e}^*] \tag{1.21}$$

Since $\mathbf{e} \perp \nabla L$, the equation becomes

$$\langle \mathbf{S} \rangle = \frac{c}{2\mu}(\mathbf{e} \cdot \mathbf{e}^*)\nabla L \tag{1.22}$$

Remembering that the electric energy density $u_e$ for a monochromatic wave is given by

$$\langle u_e \rangle = \frac{\epsilon}{4}(\mathbf{e} \cdot \mathbf{e}^*) = \frac{\langle u \rangle}{2} \tag{1.23}$$

where $u$ is the time average of the total energy density of the field and also making use of the relation $n^2 = \epsilon\mu$ and $n = c/v$ the expression for the Poynting vector takes the form

$$\langle \mathbf{S} \rangle = v\langle u \rangle \frac{\nabla L}{n} \tag{1.24}$$

We can identify $\nabla L/n$ from the eikonal equation (1.19) as the unit vector normal to a surface of equal path length. Such surfaces are called *geometrical wave fronts* and we can see that the average Poynting vector is normal to them.

### 1.2.1 Limits of geometrical optics

It is crucial that we now emphasize on the limits of geometrical optics. The eikonal equation derived is based on the approximation that for $\lambda \to 0$ the right hand side of both (2.14) and (2.15) vanishes. Such an approximation is valid only if the amplitudes $\mathbf{e}$, $\mathbf{h}$ are slowly varying functions of position over domains whose linear dimensions are of the order of the wavelength. For example the boundaries of shadows or the neighbourhood of a focus are regions where geometrical optics cannot describe the behaviour of the field correctly. Furthermore phenomena of interference, diffraction or polarization are not taken into account since they depend on wave-like properties of light.

## 1.3 Ray equation

Light rays can now be defined as trajectories orthogonal to the geometrical wave front where $L = constant$. Assuming that $s$ is the arc length along the ray's curve and $\mathbf{r}$ is the position vector of a point on it and $d\mathbf{r}/ds$ is the unit tangent vector then the eikonal equation becomes

$$\nabla L = n\frac{d\mathbf{r}}{ds} \tag{1.25}$$

A differential equation can be derived in order to specify the rays in terms of the refractive index $n(\mathbf{r})$

$$\begin{aligned}\frac{d}{ds}\left(n\frac{d\mathbf{r}}{ds}\right) = \frac{d}{ds}\nabla L = \frac{d\mathbf{r}}{ds}\cdot\nabla(\nabla L) = \frac{1}{n}\nabla L\cdot\nabla(\nabla L)\\ = \frac{1}{2n}\nabla(\nabla L)^2 = \frac{1}{2n}\nabla n^2 \Rightarrow\\ \frac{d}{ds}\left(n\frac{d\mathbf{r}}{ds}\right) = \nabla n\end{aligned} \tag{1.26}$$

The equation (1.26) above is referred to as *ray equation* and can be used to estimate the trajectory of a ray in a medium of known refractive index distribution. As an example, let's consider the case of homogeneous medium. In this case the refractive index is constant $n(\mathbf{r}) = const \Rightarrow \nabla n = 0$ so the ray equation becomes

$$\frac{d^2\mathbf{r}}{d^2s} = 0 \Rightarrow \frac{d\mathbf{r}}{ds} = \mathbf{a} \Rightarrow \mathbf{r} = \mathbf{r}_0 + s\ \mathbf{a} \tag{1.27}$$

where $\mathbf{a}$, $\mathbf{r}_0$ are constant vectors. Clearly the above solution describes a line passing from a point $O$ defined by $\mathbf{r}_0$ with direction parallel $\mathbf{a}$, thus light in homogeneous media always travels in straight lines.

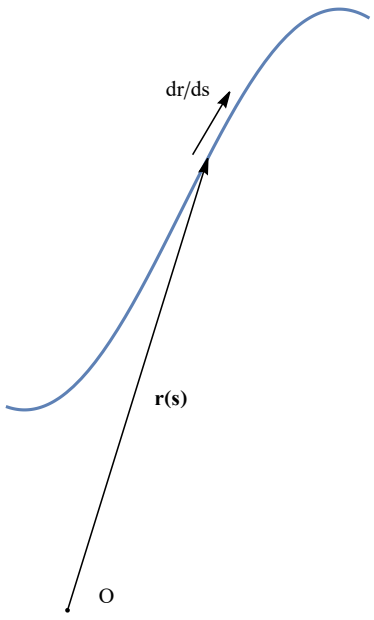


Figure 1: Curved ray in inhomogeneous medium. Here $O$ is the origin, $\mathbf{r}(s)$ is the position vector of a point on the ray and $dr/ds$ is the tangential unit vector to the ray.

# 2 Paraxial optics

Most optical systems consist of a sequence of rotationally symmetric reflecting or refracting components. The axis of symmetry is called the optical axis. Because reflected or refracted rays remain in the plain of incidence it is useful to define the meridional plane which is a plane that contains an object point $P$ and the optical axis. The plane perpendicular to the meridional plane is called sagittal plane and the rays lying on these planes are called meridional and sagittal respectively. From here on, we define the $z$ axis as the optical axis and the the $x - z$ plane as the meridional plane. Due to symmetry, rays lying on the meridional plane are sufficient to fully analyze rotationally symmetric and one-dimentional optical systems.

For rays that lie on the meridional plane, the starting positions can be determined only by their distance $x$ from the optical axis provided that the object point $P$ is at $z = 0$. So far we have reduced the six scalar parameters of $\mathbf{a}, \mathbf{r}_0$ needed to describe a ray to three, namely $(x, a_x, a_z)$. The direction vector components can be defined relative to the optical axes as $(a_x = sin\phi, a_z = cos\phi)$. Further simplifications can be made considering rays that fulfil the following conditions :

- The distance $x$ is small compared to the focal length of each optical element in the system.
- The angle $\phi$ between the ray and the optical axis as well as reflection and refraction angles have to be small i.e $\phi << 1$.

For $\phi << 1$, $a_z = cos\phi \approx 1$, $a_x = sin\phi \approx \phi$. So in the paraxial approximation only two parameters are needed and can be represented as components of a vector, the ray height $x$ and the ray $NA = n\ \phi$, where $n$ refers to the refractive index:

$$\begin{pmatrix} x \\ n\ \phi \end{pmatrix}$$

The effect of the optical system on a ray can now be viewed as a $2 \times 2$ matrix operation on the ray vector.

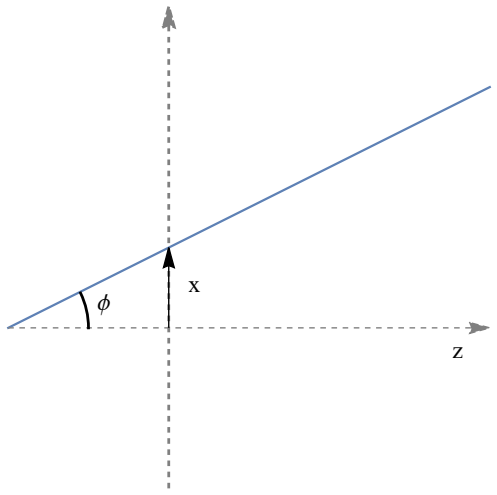


Figure 2: Parameters of paraxial theory for ray.

## 2.1 ABCD matrix theory

In order to better understand the representation of an optical system by a $2 \times 2$ matrix we will examine the case of refraction from a spherical surface where $n' > n$. As shown in Fig. 3 a ray propagates from left to right. The center $C$ of the spherical surface lies on the optical axis is the z axis, and $V$ is the vertex and $P$ is the intersection point respectively. The angles between the surface normal **PC** and the incident and refracted ray are $i$, $i'$ respectively while the angles with the optical axis are $\phi$ and $\phi'$.
We can see that

$$\phi + \alpha = i, \;\; \phi' + \alpha = i'$$

From Snell's law we know that

$$n \sin(i) = n' \sin(i')$$

In the paraxial approximation the incidence and refraction angles are small so $\sin(i) \approx i$ and we have

$$n \; i \approx n \; i'$$

Also for small distances $x$ from the optical axis we have

$$sin(\alpha) = \frac{x}{R} \Rightarrow \alpha \approx \frac{x}{R}$$

These expressions allow us to express the angle $\phi'$ as a function of the surface and incident ray parameters:

$$n'\phi' = n\phi - \frac{n' - n}{R} x$$

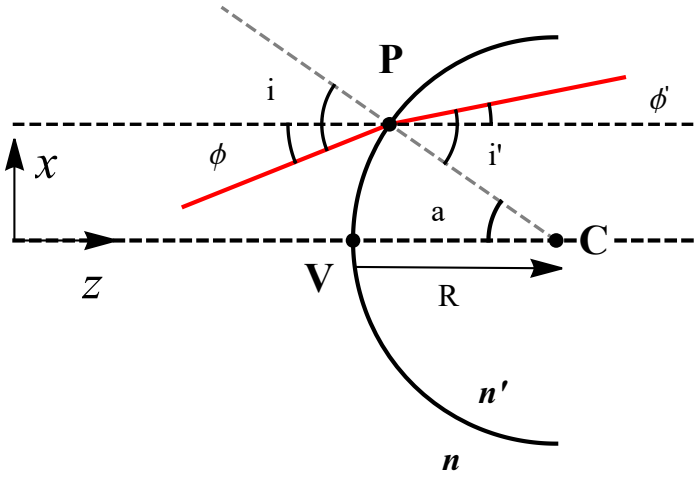


Figure 3: Refraction from a spherical surface

Taking into account that the ray height does not change in the case of refraction the matrix $M_f$ is defined as:

$$\begin{pmatrix} x' \\ n'\phi' \end{pmatrix} = \begin{pmatrix} 1 & 0 \\ -\frac{n'-n}{R} & 1 \end{pmatrix} \begin{pmatrix} x \\ n\phi \end{pmatrix}$$

Similarly the matrices for reflection $M_l$ from a spherical surface and propagation between two perpendicular to the optical axis planes of distance $d$ $M_t$ can be defined as

$$M_l = \begin{pmatrix} 1 & 0 \\ \frac{2n}{R} & 1 \end{pmatrix}, M_t = \begin{pmatrix} 1 & \frac{d}{n} \\ 0 & 1 \end{pmatrix}$$

Matrices for refraction or reflection from plane surfaces are the limiting cases $R \to \infty$.

Furthermore, any rotationally symmetric optical system consisting of a sequence of refractive or reflective elements can be defined by a matrix $M_T$ which is the product of a sequence of matrices.

$$M_T = M_i M_{i-1} M_{i-2} .... M_1 = \begin{pmatrix} A & B \\ C & D \end{pmatrix}$$

where $i$ denotes the order by which the elements are intercepted by the ray. The sign conventions for the paraxial matrix theory are the following:

- Ray angles $\phi$ are positive when $\sin\phi > 0$.
- Ray heights are upward positive.
- Radii of curvature are positive if the center of curvature is at the right of the vertex of the surface.
- Light rays travel from left to right for positive distances $d$. Negative propagation distances means that rays travel from right to left.
- When light travels from right to left the refractive index is set as negative $n < 0$.

## 2.2 Optical Systems

At this point the term optical imaging has to be explained. In an ideal imaging system all the rays coming from an object point passing through the system intersect each other on the other side at a single point thus forming the object point's image. In most practical systems this in not the case since aberrations are present but within the limits of the paraxial approximation perfect imaging is possible. The paraxial theory though remains usefull since properties of an optical system can be robustly defined.

At first the lateral magnification of the system $\beta$ can be defined as the ratio of image height to object height

$$\beta = \frac{x_I}{x_O}$$

Furthermore another kind of magnification, angular magnification can be defined as the ratio of the angle the ray makes with the optical axes at the image space to the angle in the object space

$$\gamma = \frac{\tan \phi'}{\tan \phi} \approx \frac{\phi'}{\phi}$$

Other important properties defined with the help of paraxial theory are the so called cardinal points of the system comprised by the principal planes, the focal points and the nodal points. In the following, each one will be considered so that their importance is understood.

Principal planes: An object point at the principal plane $\mathcal{U}$ of the object space is imaged at the principal plane $\mathcal{U}'$ of the image space with lateral magnification $\beta = +1$. The key property here being that a ray intersecting the plane $\mathcal{U}$ at a height $x$ also intersects $\mathcal{U}'$ with the same height allowing us to construct the ray path graphically.Likewise, the points of intersection of those planes with the optical axes are called principal points $U$,$U'$.

Focal points: The focal points $F$ (in the object space) and $F'$ in the image space have the following properties. A ray starting from $F$ is transformed into a ray parallel to the optical axis in the image space. Vice versa, a ray parallel to the optical axis in the object space intersects $F'$ in the image space. The planes perpendicular to the optical axis that contain $F$, $F'$ are called focal planes. The distance between $F$ and $\mathcal{U}$ is called the focal length $f$ in the object space and the distance between $F'$ and $\mathcal{U}'$ is called the focal length $f'$ in the image space. The sign convention is that $f$ is positive if the focal point is located at the right/left of the principal point in the image/object space. The key property here being that rays with object height $x$ in the object space form a bundle of parallel rays in the image space making an angle $\phi' = -x_O/f'$ with the optical axis.

Nodal points: The nodal points of an optical system $N$ (in the object space) and $N'$ (in the image space) are the points of intersection of a ray with the optical axis where $\phi = \phi'$. At $N$, $N'$ the angular magnification is $\gamma = 1$.

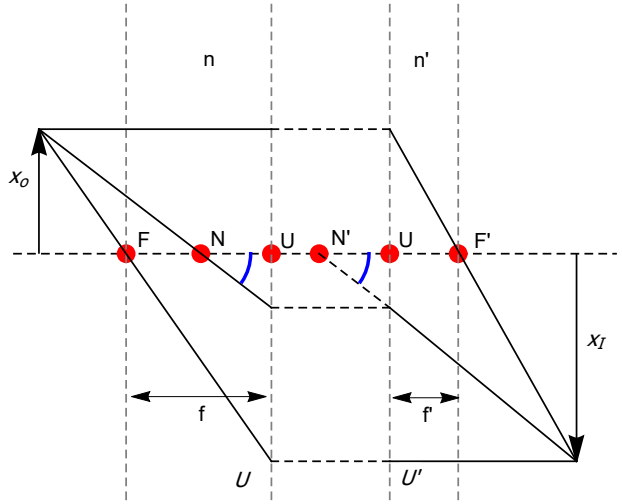


Figure 4: Cardinal points of an optical system

Cardinal points of an optical system control image location and magnification. On the other hand, another important feature is image illumination. The image can be bright or dim or unevenly bright in the center compared to the edges. Such image characteristics are controlled by the size and location of specific apertures in the system. In the following we will briefly describe the most important of them.

Aperture stop: The aperture stop of an optical system limits the angular breadth of the rays that come from an axial object and as result affects the illumination of the image. It can be found when all the apertures of the system are imaged in the object space. This includes any physical stops or the rims of the optical elements. It is worth mentioning that a ray that passes through the center of the aperture stop is called a chief ray and rays that pass through the edges of the aperture stop are called marginal rays. Both provide a simple way to examine the imaging properties of an optical system.

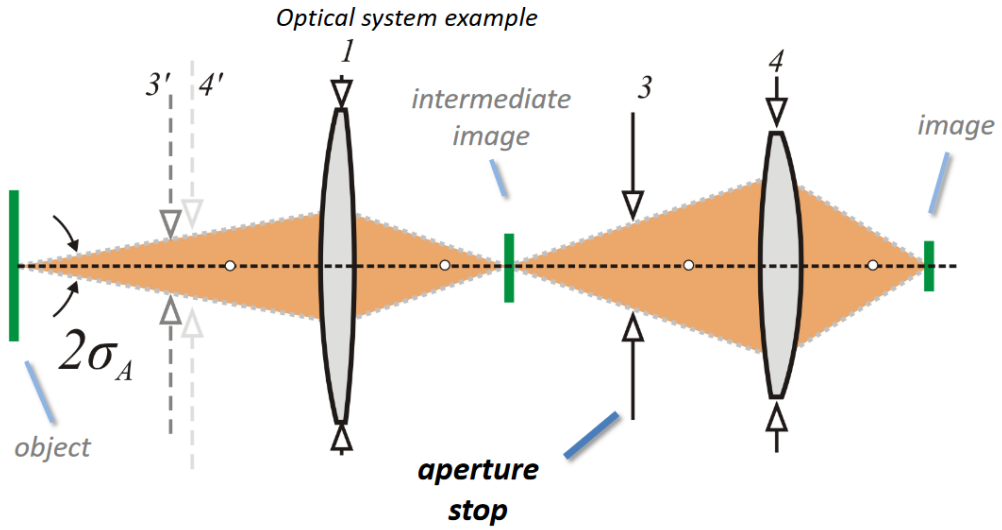


Figure 5: Entrance and exit pupils of an optical system. [9]

Entrance and exit pupils: The entrance pupil of an optical system is defined as the image of the aperture stop in the object space. On the other hand, the exit pupil of the optical system is defined as the image of the aperture stop in the image space. The importance of the entrace and exit pupils lies in the fact that they provide a way to investigate how rays coming from off axis angular positions are affected by the apertures and the optical elements of the system.

## 2.3 Telescopic systems

One of the most important optical systems is the telescope with many applications in optics as well as astronomical observations. The telescope is an afocal optical system meaning that its focusing power is zero and so its focal length lies at infinity. That being said, parallel rays entering the system emerge parallel from the exit. Although a common believe is that afocal optical systems are used only in astronomy, or for observation of far away objects, they can also be used to image objects at a finite distance. In this case they are referred to as *telecentric systems* and one of they unique properties is that the image magnification is

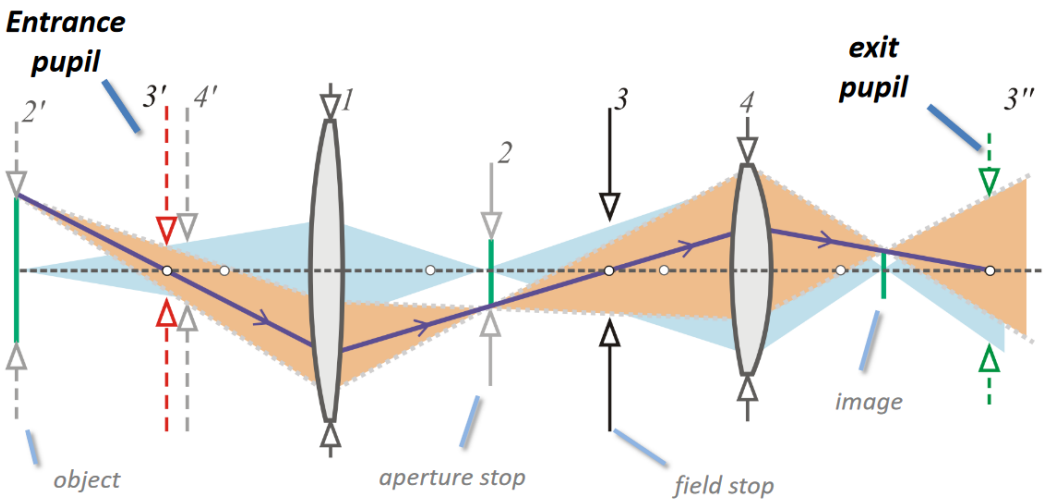


Figure 6: Entrance and exit pupils of an optical system. [9]

constant and does not depend on object position. An afocal optical system is described by an matrix of the the form :

$$M^{tel} \equiv \begin{pmatrix} M_{11} & M_{12} \\ 0 & M_{22} \end{pmatrix}$$

Thus an afocal system has no optical power $M_{21}^{tel} \equiv 0$. Using the $ABCD$ matrix formulation we have for the input and output ray angles:

$$n'\phi' = M_{21}x + M_{22}\ n\phi = M_{22}\ n\phi \Rightarrow \phi' = \frac{n}{n'}M_{22}\phi$$

Thus rays that are parallel entering the optical system emerge parallel. In the case that the medium in the object and image space is the same $n' = n$ then the element $M_{22}$ is the angular magnification.

As an example we will consider a two lens optical system situated in air to demonstrate its principles.

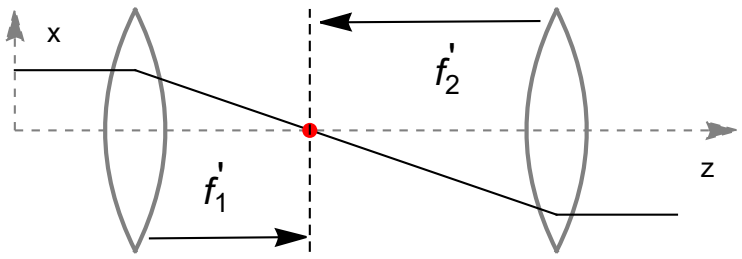


Figure 7: Telescopic system set up

The paraxial matrix $M$ from $\mathcal{U}_1$ to $\mathcal{U}'_2$ is :

$$M = \begin{pmatrix} 1 & 0 \\ -1/f'_2 & 1 \end{pmatrix} \cdot \begin{pmatrix} 1 & d \\ 0 & 1 \end{pmatrix} \cdot \begin{pmatrix} 1 & 0 \\ -1/f'_1 & 1 \end{pmatrix}$$

$$M_{21} = -1/f_1' - 1/f_2' + d/f_1'f_2' = 0$$
$$\Rightarrow d = f_1' + f_2'$$

So the matrix takes the form:

$$M = \begin{pmatrix} -\frac{f_2'}{f_1'} & f_1' + f_2' \\ 0 & -\frac{f_1'}{f_2'} \end{pmatrix}$$

We can see that the angular magnification is

$$\gamma = \frac{\phi'}{\phi} = -\frac{f_1'}{f_2'}$$

As a result the size of the image of a far-distant object only depends on the ratio of the focal lengths.

Another key property of telecentric systems is that they increase or decrease the width of a collimated beam. To showcase this beam expanding property lets consider, two parallel rays ($\phi_1 = \phi_2$) of different height $x_1 \neq x_2$. If we denote their initial separation by $\Delta x$ we can calculate their displacement at the exit as follows:

$$\Delta x' = x_2' - x_1' = -\frac{f_2'}{f_1'}\Delta x = \frac{\Delta x}{\gamma}$$

We can see that their separation explicitely depends on the angular magnification so the beam expanding ratio is:

$$\frac{\Delta x'}{\Delta x} = \frac{1}{\gamma}$$

# 3 Beyond paraxial approximation

In the paraxial case the imaging quality of an optical system is ideal, meaning that all rays from an object point converge to a single image point. This is a somehow idealized behaviour and in reality most systems do not exhibit ideal imaging the image is deformed and deteriorated. Such distortions of the image are collectively called aberrations. The effects of aberrations can be studied either numerically by exact tracing of a ray through the optical system by an approach referred to as *ray tracing* or by algebraic means namely aberration theory. Both approaches will be considered in the following section.

## 3.1 Optical aberrations

There are two types of aberrations monochromatic and chromatic. Monochromatic aberrations are due to the geometry of the system's surfaces as well as their placement in space. In the case of monochromatic aberrations we can either study the failure of the output wavefront to converge into a single point (wavefront aberration) or the displacement of a ray with respect to its paraxial image point (ray aberration). On the other hand, chromatic aberrations result from the effect of dispersion, i.e. the dependence of refractive index on wavelength. Chromatic aberrations appear also in paraxial optical systems where for example can affect the position of the focal points.

Ray aberration: For a rotationally symmetrical optical system, let $P_0'$,$P_1'$,$P_1$ be the points in which a ray from an object point $P_0$ intersects the plane of the entrance pupil, the exit pupil and the paraxial image plane respectively. If $P_1^*$ is the paraxial image point of $P_0$ the vector $\boldsymbol{\delta} = P_1^* P_1$ is called the ray aberration.
Wave aberration: Let $W$ be the wavefront through the centre $O_1'$ of the exit pupil, associated with the image-forming pencil of rays which reaches the image space from $P_0$. In the absence of aberrations, $W$ coincides with a sphere $S$ which is centred on the paraxial image point $P^*$ and which passes through $O_1'$ : $S$ will be called the paraxial reference sphere.

Let $Q$ and $\bar{Q}$ be the points of intersection of the ray $P_1' P_1$ with the paraxial reference

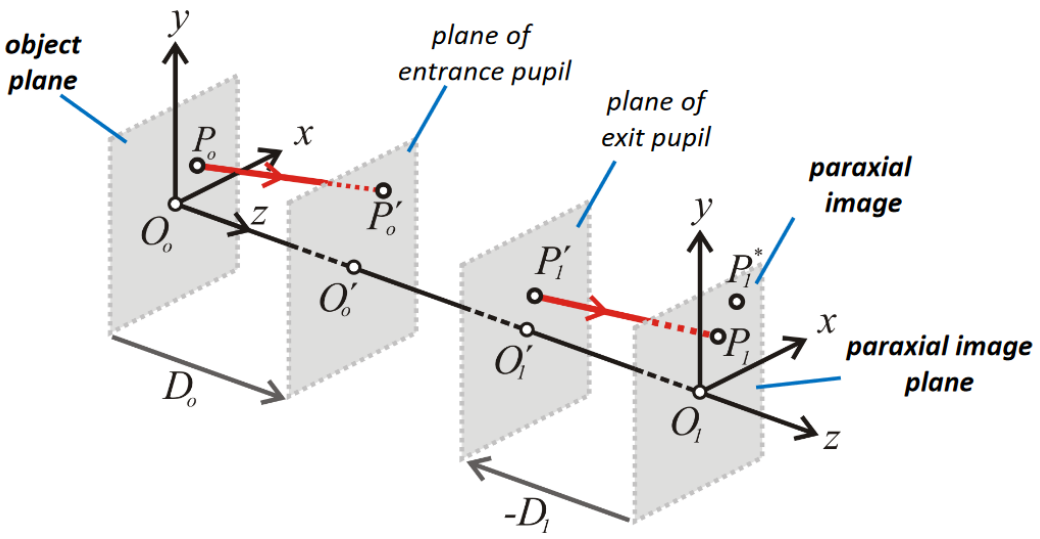


Figure 8: Object, image and pupil planes. [9].

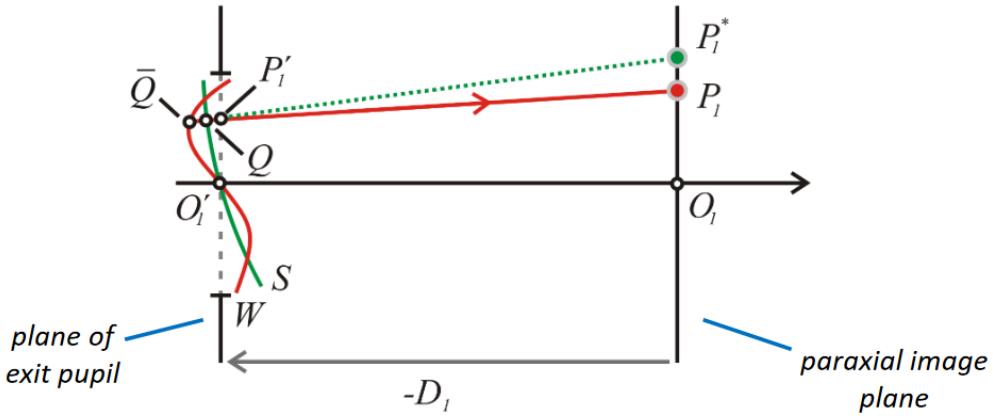


Figure 9: Wave aberration [9]

sphere and with the wavefront $W$ respectively. The optical path length $\Phi = [\bar{Q}Q]$ may be called the aberration of the wave element at $Q$, or simply the wave aberration, and will be regarded as positive if $\bar{Q}$ and $P_1$ are on the opposite sides of $Q$. In typical commercial optical systems, the wave aberrations may be as much as forty or fifty wavelengths in strength, but in instruments used for more precise work (such as astronomical telescopes or microscopes) they must be reduced to a much smaller value, only a fraction of a wavelength.

## 3.2 Seidel aberrations

The wave aberration function $\Phi(\rho, \theta, y_0)$ of an optical imaging system with an axis of rotational symmetry depends on the object height $y_0$ from the optical axis and pupil coordinates $(\rho, \theta)$ of a point in the plane of the exit pupil through three rotational invariants $y_0^2$, $\rho^2$, $y_0 \rho cos\theta$. Since the wave aberration function has to be rotationally invariant we can expand $\Phi$ in polynomials of degree $2k$ in the coordinates.

$$\Phi = \Phi^{(0)} + \Phi^{(4)} + ... + \Phi^{(2k)} \tag{3.1}$$

The aberrations of lowest order $2k = 4$ are called *primary* or *Seidel aberrations*. They depend on the rotational invariants as [3]:

$$\Phi^{(4)} = -\frac{1}{4}B\rho^4 - Cy_0^2\rho^2 cos^2\theta - \frac{1}{2}Dy_0^2\rho^2 + Ey_0^3\rho cos\theta + Fy_0\rho^3 cos\theta \tag{3.2}$$

where $B$ relates to the strength of spherical aberration, $C$ to astigmatism, $D$ to field curvature, $E$ to distortion and $F$ to coma aberration.Likewise, the ray aberration can be expressed as a function of the exit pupil coordinates:

$$\boldsymbol{\delta} = \Delta x(y_0, \rho, cos\theta)\hat{\mathbf{x}} + \Delta y(y_0, \rho, cos\theta)\hat{\mathbf{y}} \tag{3.3}$$

$\boldsymbol{\delta}$ can be estimated using the wave aberration coefficients using the approximate relations [10]:

$$\frac{\partial \Phi}{\partial x} = -\frac{\Delta x}{R}, \frac{\partial \Phi}{\partial y} = -\frac{\Delta y}{R} \tag{3.4}$$

So 4.2.2 takes the form

$$\Delta^{(3)}x = B\rho sin\theta - 2Fy_0\rho^2 sin\theta cos\theta + Dy_0^2\rho sin\theta$$
$$\Delta^{(3)}y = B\rho cos\theta - 2Fy_0\rho^2(1 + 2cos^2\theta) + (2C + D)y_0^2\rho cos\theta - Ey_0^3 \tag{3.5}$$

In the special case when all the coefficients in Eq. 4.2 have zero values, the wave-front in the exit pupil coincides, within a degree of accuracy, with the paraxial reference sphere. In general, the aberration coefficients will have finite values. Each term then represents a particular type of departure of the wave-front from the ideal spherical form. The curves traced out in the image plane by the intersection points of all the rays emerging from a fixed zone $\rho = const.$ of the exit pupil are called aberration curves and help illustrate them graphically.

Spherical aberration (SA): When all coefficients except $B$ are zero, the $3^{rd}$ order ray aberrations become

$$\Delta^{(3)}x = B\rho^3 sin\theta$$
$$\Delta^{(3)}y = B\rho^3 cos\theta \tag{3.6}$$

The aberration curves are in this case concentric circles whose centres are at the paraxial image point and whose radii increase with the third power of the zonal radius, but are independent of the object height $y_0$. This defect of the image is called *spherical aberration* and manifests even for paraxial objects, without affecting the beam's symmetry. If a screen is placed in the image region at right angles to the axis, there is a position for which the circular image spot appearing on the screen is a minimum; this minimal 'image' is called the circle of least confusion. As shown in Fig. 10, in a system that suffers from spherical aberration the focal point depends on the position of the ray in the exit pupil. As rays approach to the rim of the lens the focal distance decreases (in absolute value).

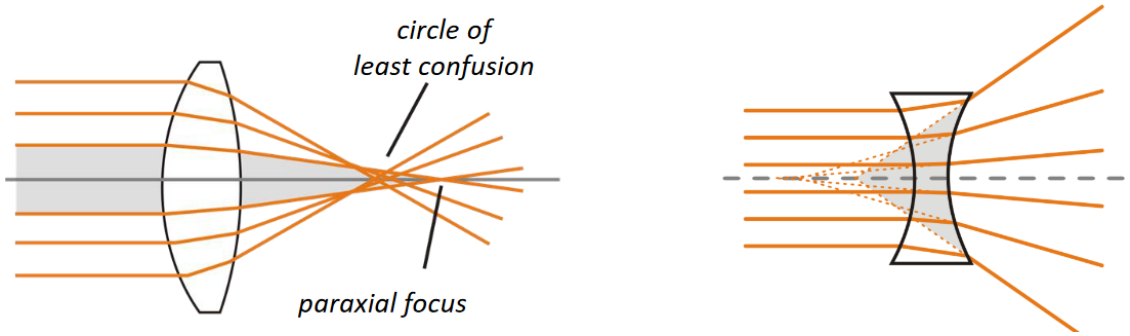


Figure 10: Spherical aberration [9]

Comma aberration (CA): When all coefficients except $F$ are zero, the 3rd order ray aberrations become :

$$\Delta^{(3)}x = -Fy_0\rho^2 sin2\theta$$
$$\Delta^{(3)}y = -Fy_0\rho^2(2 + cos2\theta) \tag{3.7}$$

Now if $y_0$ is fixed and the zonal radius $\rho$ is kept constant, the point in the image plane describes a circle twice over as $\theta$ runs through the range $[0, 2\pi]$. The circle is of radius $|Fy_0\rho^2|$ and its centre is at a distance $-2F\rho^2 y_0$ from the paraxial image point, in the $y$-direction. The circle therefore touches the two straight lines which pass through the paraxial image and which are inclined to the $y$ axis at 30°. As $\rho$ takes on all possible values, the circles cover a region bounded by segments of the two straight lines and by an arc of the largest aberration circle. The overall size increases linearly with the off axis distance of the object point.

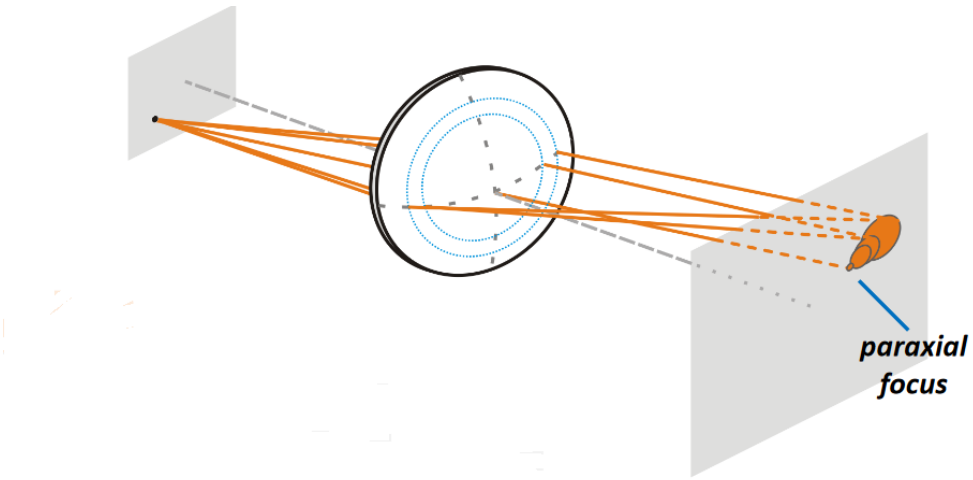


Figure 11: Comma aberration [9]

Distortion (DS): When all coefficients except $E$ are zero the 3rd order ray aberrations become :

$$\begin{aligned} \Delta^{(3)}x &= 0 \\ \Delta^{(3)}y &= -Ey_0^3 \end{aligned} \tag{3.8}$$

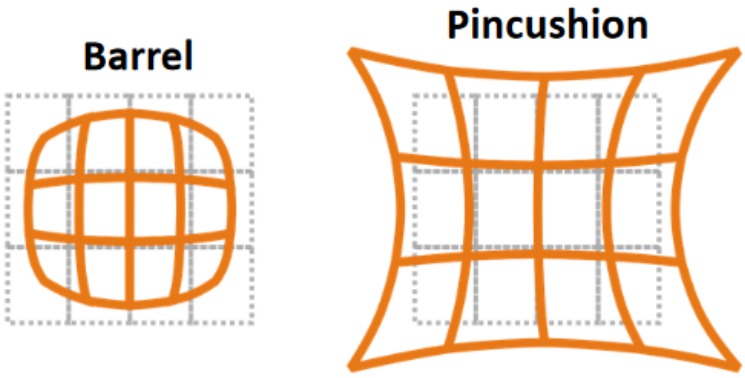


Figure 12: Barrel and pincushion distortion [9]

Because the the ray aberrations are independent of $\rho$ and $\theta$ the imaging will be stigmatic and independent of the pupil radius. The transverse magnification of the image will however

will depend on the object height $y_0$. This aberration thus results in a geometric distortion of the image. As shown in Fig. 12, depending on the sign of $E$ we can have two types of distortion , barrel ($E > 0$) and pincushion ($E < 0$), while the image of straight lines, except of those that cross the optical axis will be curved.

Astigmatism (AS): When all coefficients except $C$ are zero the 3rd order ray aberrations become:

$$\begin{aligned} \Delta^{(3)}y &= 2C\rho y_0^2 cos\theta \\ \Delta^{(3)}x &= 0 \end{aligned} \tag{3.9}$$

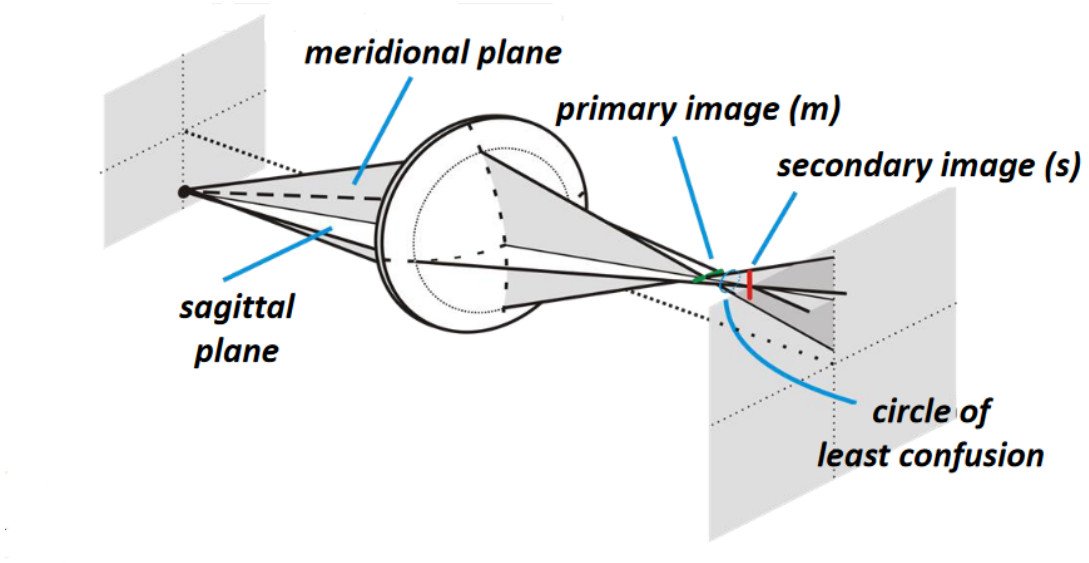


Figure 13: Astigmatism in the case of the meridional and sagittal plane.[9]

In the case of astigmatism rays that propagate in mutually perpendicular planes have different foci. For example, as shwon in Fig. 13, lets consider the sagittal and meridional planes for the case of an off axis object point. Rays that lie on these two planes will focus at two different foci that are separated by a distance $l$ referred to as the *astigmatic focal distance*. In between the foci there is a plane representing the best compromise image location in a system with astigmatism called the *circle of least confusion*.

Field curvature (FC): When all coefficients except $D$ are zero the 3rd order ray aberrations become:

$$\begin{aligned} \Delta^{(3)}x &= D\rho y_0^2 sin\theta \\ \Delta^{(3)}y &= D\rho y_0^2 cos\theta \end{aligned} \tag{3.10}$$

In presence of field curvature, an object segment in the object plane is stigmatically imaged on a curved surface. This surface is known as the *Petzval surface*. In the presence of

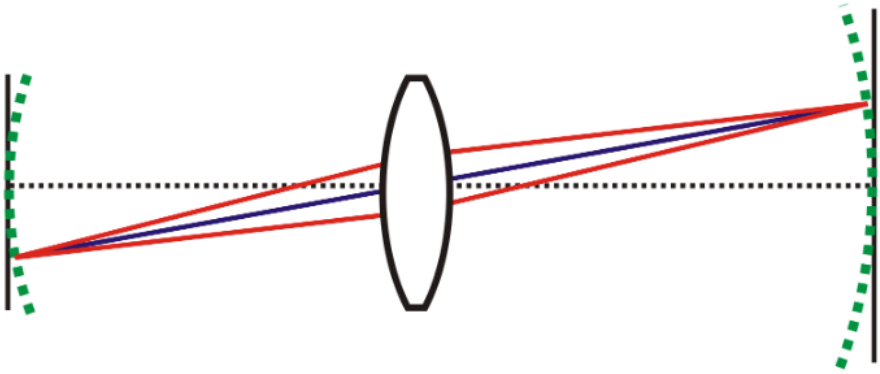

Figure 14: Field curvature for an optical system of one lens. [9]

astigmatism the *Petzval surface* splits into two surfaces, the primary (related to the meridional plane) and the secondary (related to the sagittal plane).

An example of the effect of (FC) in the image of a cross-hair object, when a flat screen is placed on the paraxial image plane, is shown in Fig. 15(a). As we can clearly see in the image is in sharp focus at its center and blurred at the edges. On the other hand, when we move the flat screen closer to the lens, as shown in Fig. 15(b), the edges are in focus while the center becomes blurred.

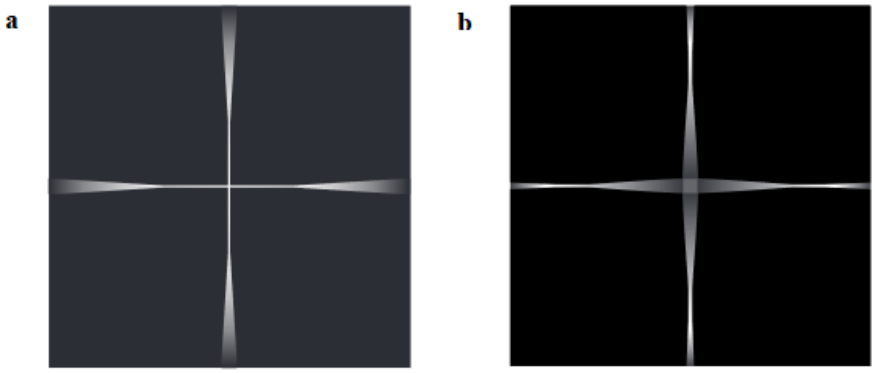


Figure 15: Effect of field curvature. Image of a cross-hair object when the screen is placed (a) at the paraxial focus, (b) shifted closer to the lens [6]

## 3.3 Zernike polynomials

The Zernike polynomials are a set of orthogonal polynomials on the unit disk ( defined as the set of points with radial distance less than unit). There are even and odd Zernike polynomials. The even Zernike polynomials are defined as :

$$Z_n^m(\rho,\phi)_o = R_n^m(\rho)cos(m\phi)$$

The odd Zernike polynomials are defined as:

$$Z_n^m(\rho,\phi)_e = R_n^m(\rho)sin(m\phi)$$

where $\phi$ is the azimuthal angle, $\rho$ is the radial distance $0 \leq \rho \leq 1$ and $n$, $m$ are non-negative integers $n \geq m \geq 0$, and $R_n^m$ are the radial polynomials defined as :

$$R_n^m(\rho) = \begin{cases} \sum_{l=0}^{\frac{n-m}{2}} \frac{(-1)^l (n-l)!}{l!\left(\frac{1}{2}(n+m)-l\right)!\left(\frac{1}{2}(n-m)-l\right)!} \rho^{n-2l} & \text{for } n-m \text{ even} \\ 0 & \text{for } n-m \text{ odd} \end{cases}$$

Any sufficiently smooth real valued function $W(\rho, \phi)$ can by be represented in terms of its Zernike coefficients.

$$W(\rho, \phi) = \sum_{m=0}^{\infty} \sum_{n=m}^{\infty} [A_n^m Z_n^m(\rho, \phi)_o + B_n^m Z_n^m(\rho, \phi)_e]$$

where the coefficients $A_n^m,\ B_n^m$ are given by

$$A_n^m = \frac{(n+1)}{\epsilon_{mn}^2 \pi} \int_0^1 \int_0^{2\pi} W(\rho, \phi) Z_n^m(\rho, \phi)_o \rho d\phi d\rho$$
$$B_n^m = \frac{(n+1)}{\epsilon_{mn}^2 \pi} \int_0^1 \int_0^{2\pi} W(\rho, \phi) Z_n^m(\rho, \phi)_e \rho d\phi d\rho$$

and $\epsilon_{mn}$ is defined by

$$\epsilon_{mn} = \begin{cases} \frac{1}{\sqrt{2}} & \text{for } m = 0, n \neq 0 \\ 1 & \text{otherwise} \end{cases}$$

Because the Zernike polynomials are orthogonal on the unit disk they provide a complete basis to expand wavefront functions of systems with circular pupils.Furthermore, they provide an alternative, more efficient, way to describe optical aberrations since the Seidel wave aberration terms directly correspond to specific Zernike polynomials .

Zernike polynomials are widely used in many different fields. For example, they are now routinely used in ophthalmology in order to describe wavefront aberrations of the cornea. Likewise, they are used to identify wavefront aberrations of an optical system, or in the field of adaptive optics to characterize atmospheric distortion. Furthermore, they are used to characterize higher order errors observed in interferometric analysis. Zernike polynomials provide a detailed, analytic way to characterize a wavefront in contrast to other characterization methods that rely on simple averaging metrics like the $RMS$ error. For example, let's take the case of two distinctly different wavefronts that compared to an ideal spherical wavefront, may have the same $RMS$ error. By decomposing them into Zernike polynomials and calculating their coefficients each wavefront acquires a unique identity, while also quantifying the various aberration terms.

| Primary aberration | n | m | Zernike polynomial |
|---|---|---|---|
| Distortion | 1 | 1 | $\rho cos\theta$ |
| Field Curvature | 2 | 0 | $2\rho^2 - 1$ |
| Spherical | 4 | 0 | $6\rho^4 - 6\rho^2 + 1$ |
| Coma | 3 | 1 | $(3\rho^3 - 2\rho)cos\theta$ |
| Astigmatism | 2 | 2 | $\rho^2 cos2\theta$ |

Table 1: Primary Seidel Aberrations and Zernike Polynomials

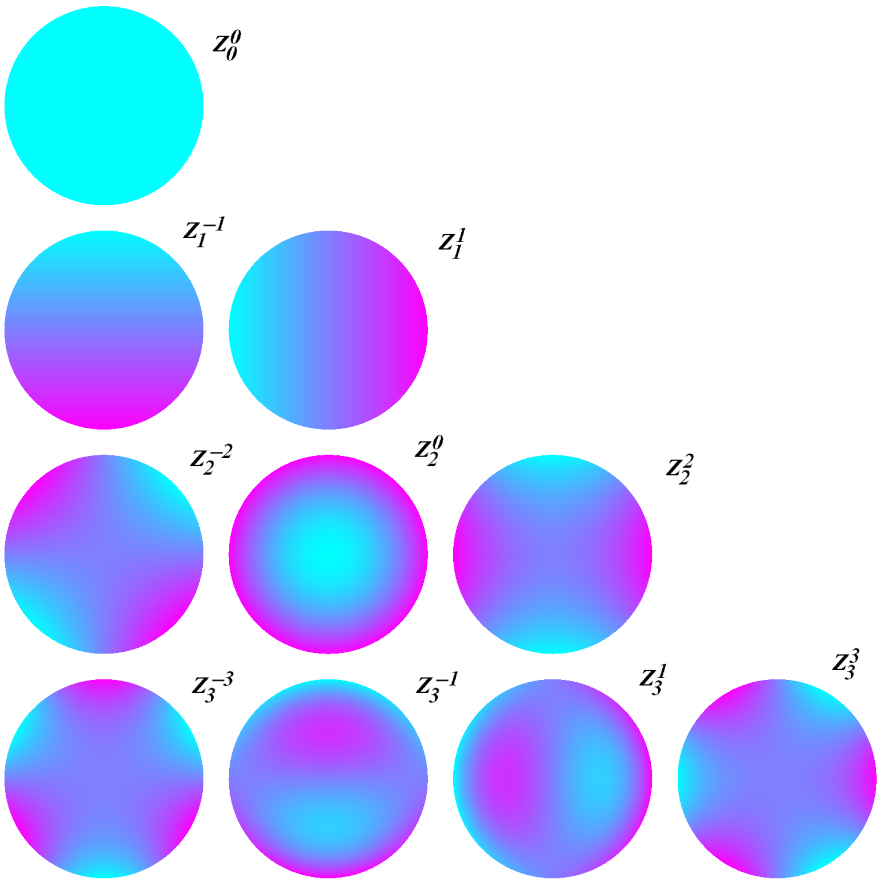


Figure 16: The first 10 Zernike polynomials ordered vertically by radial degree and horizontally by azimuthal degree.

## 3.4 Ray tracing

We have seen that as long as the geometrical optics approximation is valid light propagation can be described by rays. The procedure of keeping track of a ray's origin and direction as it travels through an optical system is called *ray tracing*. This technique forms the basis of optical design and optimization or in other words *Optical Engineering*. The most valuable information ray tracing provides is the ray's position in three dimensional space. Using this information the optical path of a ray can be calculated and consequently the phase that was accumulated along the propagation. Tracing of a bundle of rays can help identify and quantify an optical system's monochromatic aberrations and even reconstruct the phase distribution, and thus the wavefront, at its exit. It enables the optical designer to optimize the configuration at hand and further control its imaging properties. Furthermore since the optical path can be deduced, tracing a beam of polychromatic light is also possible, provided that the change, due to dispersion in the refractive index of the materials involved is accounted for. As a result chromatic aberrations can also be calculated and eliminated.

For the case of homogeneous and isotropic materials, like glass lenses and mirrors, propagation is rectilinear and the law of reflection and refraction at the interface suffice in order to determine the path of rays. On the other hand, in the case of inhomogeneous media the ray equation Eq. (1.26) has to be used in order to determine the path of the ray. With the help of computers tracing a bundle of rays through an optical system can be automated

provided that all aspects and positions of each element of the system are accurately known. To elaborate the necessary preconditions are :

- Refractive indices of the materials the elements are made of and their dependence on wavelength.
- Position, orientation and ordering of the surfaces in all three space dimensions.
- Type of surface e.g parabolic, cylindrical, plane or aspheric and its geometrical characteristics e.g radius, aspheric coefficients.
- Shape and size of the surface's boundary.

Knowing the above, tracing a ray reduces to the following algorithmic procedure

1. Find the intersection point of the ray with the optical surface that follows. If the ray does not intersect the surface, or if it is absorbed, finish the tracing of the ray. Depending on the type of tracing it may be necessary to leave the ray unchanged and go to step 4. If there is an intersection point go to step 2.
2. Calculate the surface normal at the point of intersection.
3. Apply the law of reflection or refraction and find the new direction of the ray. The intersection point becomes now the starting point of the ray.
4. If there is another surface in the system go back to step 1. If there is not, end the tracing of this ray.

The simplest type of raytracing is the sequential ray tracing. In this case, the user defines the order in which the ray intersects with each surface. In a physical system though, each ray may intersect the surfaces in a different order or even intersect multiple times with a specific surface, like in the case of an optical cavity. Likewise, a ray may split into two rays, a refracted and a reflected at an interface. In such cases, the sequential algorithm fails to produce valid results and non-sequential raytracing should be used. Unlike sequential in non-sequential raytracing the intersection point of a ray with each one of the surfaces is repeatedly calculated and the path is traced based on which one is closer to the ray's starting point. Non-sequential ray tracing is used in designing illumination systems such as projector systems, collimators or LCD displays. In addition to this, non sequential raytracing plays a vital role in the stability analysis of laser optical cavities. At last it is important to note that such a practice is computationally demanding and used only if necessary.

Modern raytracing software can also perform polarization raytracing. Here the ray's polarization state is taken into account and using Fresnel equations the optical power of the reflected and refracted ray can be deduced. Furthermore, there exists yet another, less used, type of raytracing called *differential raytracing*. In this case each ray represents a local wavefront with two principal curvatures and two principal directions. These parameters are traced along with normal ray parameters for each ray during propagation. Such a method allows the calculation of local astigmatism or the change of local intensity of the wave during propagation.

## 3.5 Ray tracing software

Here we will briefly describe some of the available and commonly used ray tracing software. A brief description of their key assets accompanied with simple examples will be examined .

RayOpt: A simple, open-source ray tracing Python package. It can be used for optical design of imaging systems since it includes geometric, paraxial and gaussian ray tracing. The current distribution already contains all optical materials from http://refractiveindex.info/. External material and commercial lens catalogs can also be imported and used in the design.

Optica: An new generation optical design software that utilises the symbolic numeric and graphic capabilities of *Mathematica*. It can sequential and non-sequential raytracing, polarization ray tracing, energy calculations, and some optimization of optical systems in three dimensional space. It also performs symbolic modeling of optical systems, diffraction, interference, wavefront, and Gaussian beam propagation calculations .

An older version of the software (*Optica 1.2*) was used in this project to calculate the phase distribution at the exit of optical systems. This version, although it does not include many of the the new features, can provide basic quantitative information like ray coordinates on a specific surface or the optical path length of the rays. This functionality was further enhanced by home-built functions that enabled to retrieve phase distribution in the exit, and an iterative GUI for tuning the parameters of the optical system in order to optimize it's performance. Furthermore, ray information can be extracted in the form of data sets and further analysed by the user.

To demonstrate its capabilities we will examine a simple optical system, and quantify its transverse spherical aberration. Specifically, a diopter, comprised by a spherical interface of radius $R = 30$ mm and aperture $40 \times 40$ mm$^2$ is illuminated by a line of rays of wavelength $\lambda = 0.45$ $\mu$m starting at 20 mm away from the surface vertex spanning at a width of 30 mm. The medium prior to the spherical interface is air ($n_{air} = 1.000877$) while after is water of refractive index $n_{water} = 1.339197$.

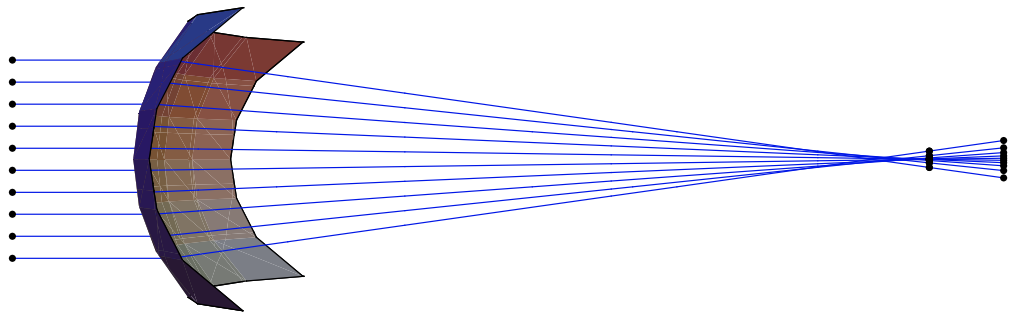

Figure 17: Refraction from a spherical surface. Raytracing performed by *Optica*

Using the paraxial matrix theory presented in Chapter 2 we can calculate the focal length of the system to be

$$f_d = \frac{n_{water} R}{n_{water} - n_{air}} = 118.751 \text{ mm}$$

measured from the vertex of the surface since the principal planes coincide at that point. The focal point can thus be calculated to be located at a position $z = f_d + 20$ mm $= 138.751$ mm.

Now that we have the focal point we can find the coordinates of the interception points of all rays with the focal plane using the ray tracer and plot their transverse displacement $\Delta y$ versus the focal plane radial distance $\rho$ and eventually find the exact form of Eq. (3.6) by fitting the data accordingly.

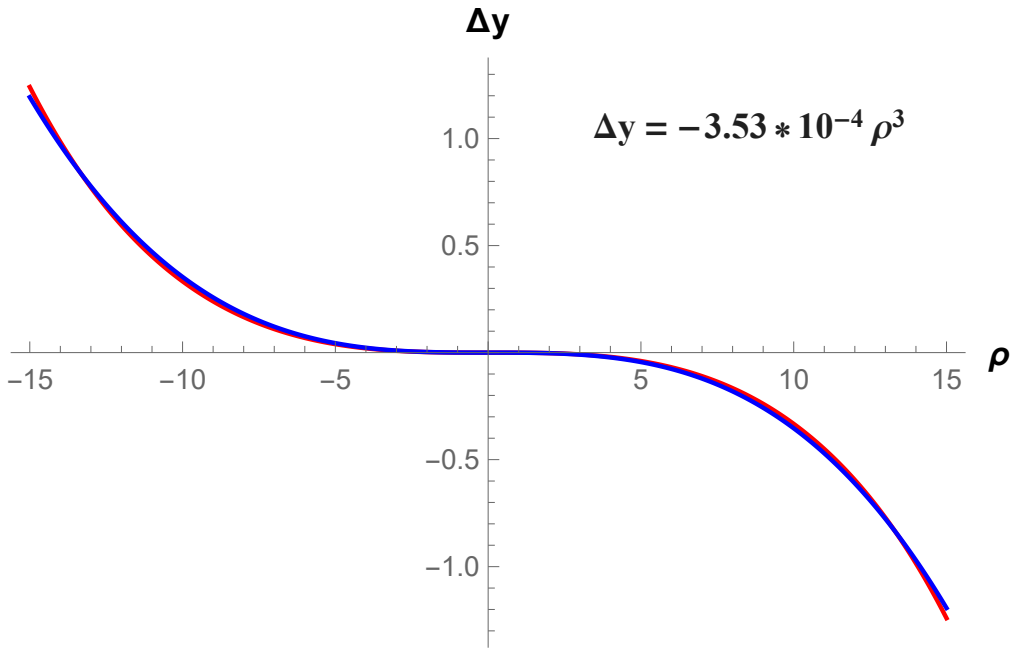


Figure 18: Transverse spherical aberration. Raytracing data (in red), Fit (in blue)

Zemax [13]: A powerful optical design software with numerous capabilities. Very complex freeform and non rotationally symmetric systems can be set up. Any kind of configuration from laser and fiber optics to illumination systems can be simulated. Zemax is also able to perform aberration analysis and optimization of set ups. Additionally thermal and polarization analysis are also included.

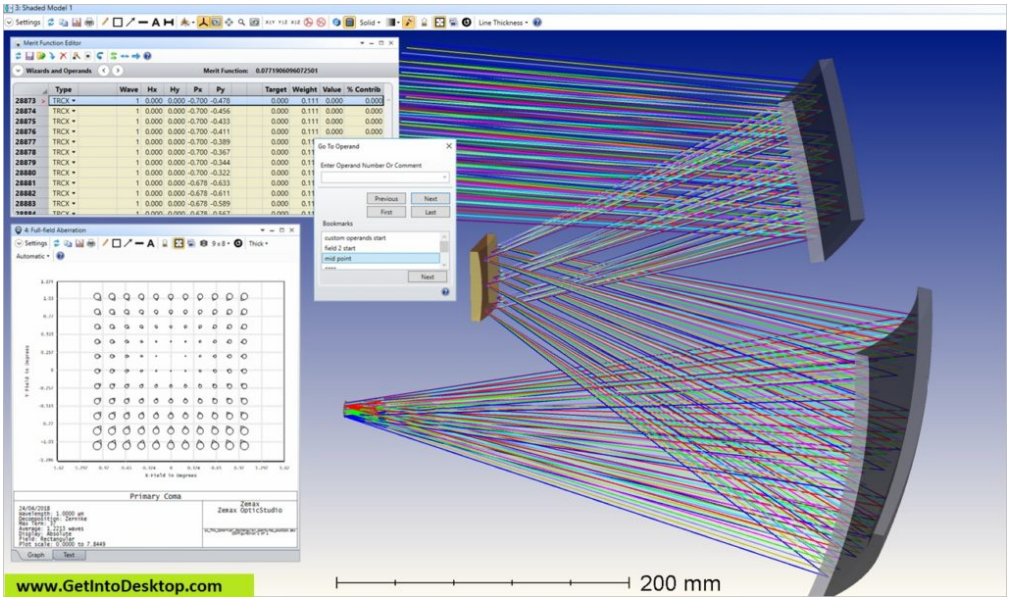


Figure 19: Screenshot from Zemax (https://www.zemax.com/)

# 4 Optical aberrations as continuous phase masks

We can envisage the wavefront aberrations that emerge in an the optical system as a smooth perturbation of the phase distribution [8, 7]. In that way, the otherwise undesirable wavefront errors acquire a new meaning. To elaborate, optical designers have always tackled the problems posed by aberrations by eliminating them to a required level. In doing so, an optimization of the optical configuration is necessary. Optical power, surface type and separation distance of the optical elements is taken into consideration in order to minimize image deterioration. Viewed in another way we may follow the optimization method in order to isolate and even maximize a specific aberration, or combine some of them in a controlled manner in order to modulate the phase field of an optical system to achieve a required optical phase distribution. Prototypes of such systems have been implemented [8, 7] and they fall into two main groups: reflective and refractive.

Refractive optical systems:
One of the refractive systems developed [8] was used to induce a pure cubic phase modulation on the wavefront of a light beam. After spatial Fourier transformation by a converging lens this lead to the generation of 1D Airy beams [12],[11], [2]. The optical design for such a device was based on the well known cylindrical beam expander. The system was comprised by two cylindrical lenses, a diverging and converging one. As shown in Fig. 20 the first lens is tilted at an angle. Without the tilt, and under paraxial approximation, a collimated beam entering a cylindrical telescope remains collimated after exiting the system. By tilting the first cylindrical lens by an angle $\phi_1$, optical aberrations are induced. A displacement of the second lens, allows the isolation minimization of all the aberrations except of the coma aberration. It is important to note that, in this system, the cubic phase modulation takes place only in the lower portion of the beam [8], as it is clearly shown in Fig. 20(a). The upper part is dominated by a strong quadratic term. So to get a net cubic phase only the lower half of the optical system is useful. In order to generate cubic phase modulation in both $x, y$ directions a second system, with orthogonal orientation, was placed after the first one, as shown in 20(b). As a result a net 2D cubic phase is achieved.

Another, relatively simpler configuration, where a pure cubic phase modulation is achieved by using only one optical element was also demonstrated [4]. In more detail, as shown in Fig. 21 a collimated beam illuminates the edge of the planar surface of a cylindrical plano-convex

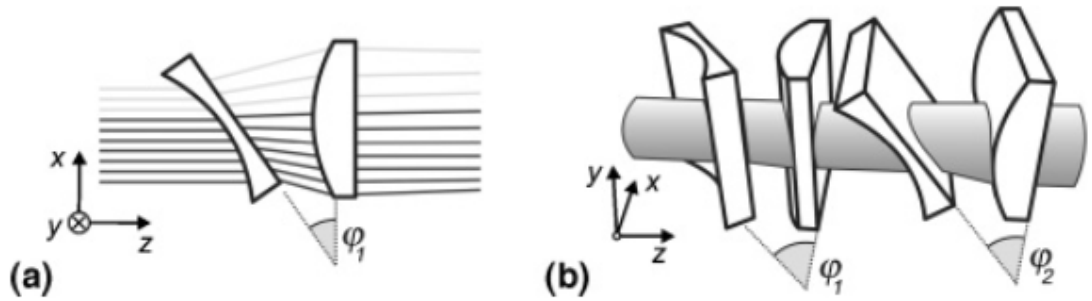


Figure 20: Tilted cylindrical 1D beam expander. (a) Generation of 1D cubic phase modulation. (b) Generation of 2D cubic phase modulation.(from [8])

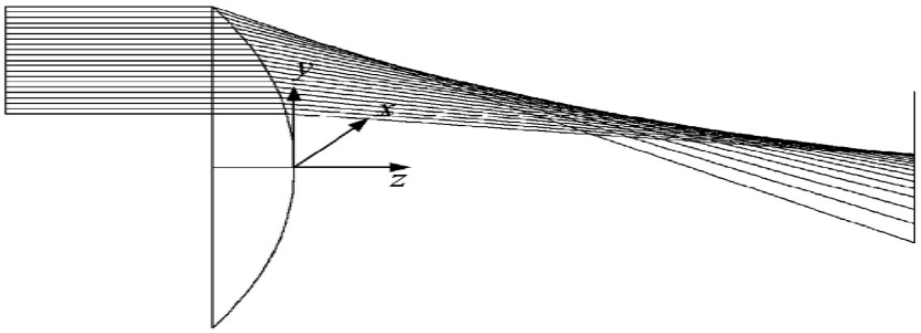


Figure 21: Raytracing result for a cylindrical lens with a decentered aperture under normal illumination. (taken from [4])

lens. Again only a part of the lens aperture (the upper part) is used in order to introduce the cubic phase term. Furthermore, although the design is considerably simpler compared to the tilted beam expander shown in Fig. 20, the wavefront in the exit is tilted in respect to the $z$ axis

Reflective optical systems:

A reflecting alternative of the refractive beam expander [8] was developed by Mansour et al. [7]. The system consisted of two cylindrical mirrors $M_1$, $M_2$ in a beam expander configuration. Following a similar strategy as in [8] aberrations were introduced by applying small variations in the orientation or the position of the optical elements. For normal incidence, light is first reflected from a convex (diverging) cylindrical mirror and then by a concave (converging) mirror. The orientation and distance between them is appropriately tuned so that the desired phase modulation is achieved. In the implementation shown in Fig. 22 an identical beam expander is placed after the first one in an orthogonal orientation in order to achieve a pure two dimensional cubic phase modulation at both transverse axes. A converging lens is then used to Fourier transform the incident Gaussian beam [5] and result to a 2D Airy beam [7].

Both of the above configurations share a common characteristic. All optical elements are of cylindrical type. Such a choice is not coincidental. Cylindrical lenses or mirrors are curved only in one direction thus they focus or defocus light only in one direction. Additionally the optical path of a beam incident on a cylindrical optical element is changed in a direction

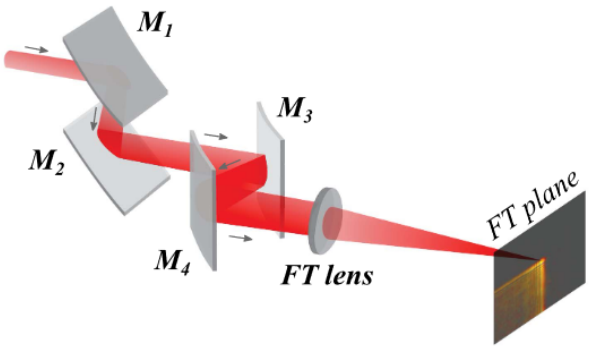


Figure 22: Representation of a reflective phase generator. (adapted from [7])

which lies in the plane of (non zero) curvature of the element and is perpendicular to the axis of propagation. It is for that reason that in order to achieve a 2D cubic phase distribution an additional system is placed orthogonally after the first in [8, 7]. The first expander produces a cubic phase distribution in the $x$ direction while leaving the $y$ direction unchanged. The second system modulates the phase in the $y$ axes while leaving the $x$ axis unchanged and overall producing a net 2D cubic phase distribution. Apart from providing a convenient way to modulate the phase for each one of the axis by just placing an exact copy of an optimized system, the cylindrical elements property to introduce aberrations only at one axis at a time also simplifies the description of the Seidel terms of wave aberrations described in Eq. (3.2), and allows for the isolation of each term. In more detail, since modulation takes place at one axis of the pupil plane i.e the $x$ axis we can safely assume that $\theta = 0 \Rightarrow cos\theta = 1$. So Eq. (3.2) becomes:

$$\Phi_{1D}^{(4)} = -\frac{1}{4}Bx^4 + Fx_0x^3 - (Cx_0^2 + \frac{1}{2}Dx_0^2)x^2 + Ex_0^3x \tag{4.1}$$

where $x_0$ is the object height and $x$ is the ray height in the exit pupil. The terms in Eq. (4.1) have been rearranged to show that the Seidel wavefront aberration terms can be seen as terms, up to the $4^{th}$ order, of a Taylor series in respect to the ray height $x$. This is only possible in the cylindrical 1D case where there is no effect of the $cos\theta$ terms that otherwise appear in (3.2). Under this perspective, the cylindrical beam expander/telescope can be viewed as the ideal template phase modulator device. Since the unperturbed beam expander is itself an afocal optical system (within the limits of the paraxial theory), a collimated beam that enters the system exits the system in that way. This means that the accumulated phase field after propagation is a constant phase bias $\Phi_0$ since each ray travels the same optical path length. Any change in the position or the orientation of the optical elements of such a system will introduce optical aberrations as described in Eq. (4.1). The optical path length traveled is not the same for each ray and depends on the ray height $x$, consequently the phase field also depends on it $\Phi = \Phi(x)$.

# 5 Reflective phase modulator

Let's now study in more detail the prototype [7] cylindrical beam expander/telescope and it's ability to modulate the spatial phase distribution of an input wavefront. As we can see in Fig. 23 the prototype system is comprised of two cylindrical mirrors $M_1$, $M_2$ in a beam expander configuration. The optical system is folded in such a way so that the chief ray in the output is parallel to the chief ray in the input, i.e. the direction of the optical axis of the system is preserved. Specifically,light is reflected by the first convex diverging mirror $M_1$ and then by the concave converging mirror $M_2$.
If $\hat{\mathbf{n}}_1$, $\hat{\mathbf{n}}_2$ are unitary vectors normal on the cylindrical surfaces, by setting $\boldsymbol{r}_1 = 0$ we have [7]:

$$\begin{aligned}
\hat{\mathbf{n}}_1 &= \cos\phi \sin\theta \ \hat{\mathbf{x}} + \sin\phi \sin\theta \ \hat{\mathbf{y}} - \cos\theta \ \hat{\mathbf{z}} \\
\hat{\mathbf{n}}_2 &= -\cos\phi' \sin\theta' \ \hat{\mathbf{x}} - \sin\phi' \sin\theta' \ \hat{\mathbf{y}} + \cos\theta' \ \hat{\mathbf{z}} \\
\boldsymbol{r}_{12} &= (\cos\phi \sin 2\theta \ \hat{\mathbf{x}} + \sin\phi \sin 2\theta \ \hat{\mathbf{y}} - \cos 2\theta \ \hat{\mathbf{z}}) \ d
\end{aligned} \tag{5.1}$$

where $d = |\boldsymbol{r}_{12}|$ is the distance between the mirrors $\theta$, $\theta' = \theta + \Delta\theta$, $\phi$, $\phi' = \phi + \Delta\phi$ are the polar and azimuthal angles of rotation of mirrors $M_1$, $M_2$ and $\Delta\theta$, $\Delta\phi$ refer to variations in the orientation of the second mirror. The system's parameters that are varied during the design are the radii of curvature $r_i$, the distance between the mirrors $d$ and the orientation of the mirrors. So setting up the beam expander geometry in a raytracing software allows us to experiment with variations of this optical setup, providing valuable insight on how phase modulation can be achieved and how the phase distribution can be tailored to fit basic functions.

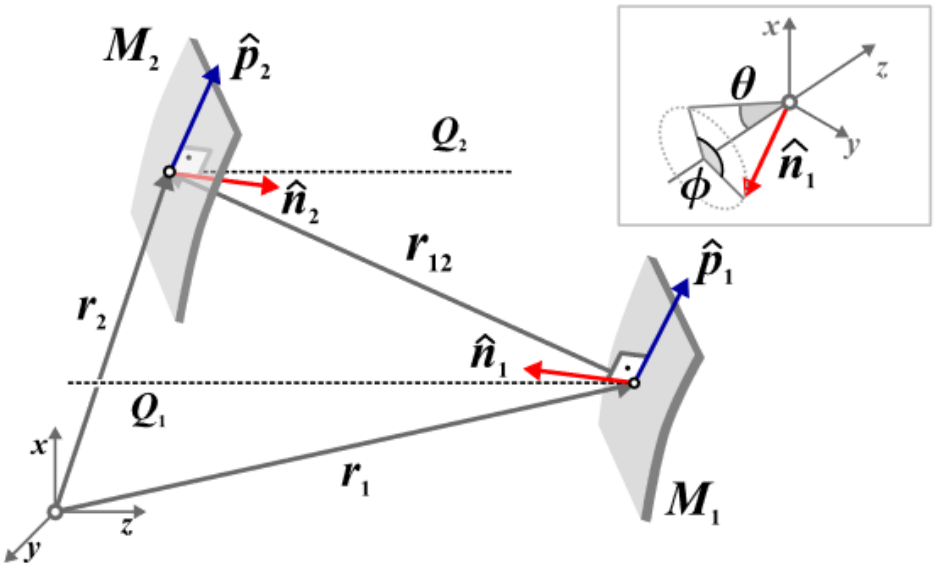


Figure 23: Cylindrical beam expander. $\hat{\mathbf{n}}_i$, $\hat{\mathbf{p}}_i$ denote the mirror orientation and direction of curvature. $Q_i$ denotes the optical axis at the entrance ($i = 1$) and the exit ($i = 2$) of the system. Inset : polar and azimuthal angles of rotation $\theta, \phi$. (adapted from [7])

## 5.1 Phase distributions

Using *Optica* we set up our cylindrical beam expander using the geometry described in Eq. (5.1). In order to manipulate the configuration we use a *GUI* (graphical user interface). Through the interface a number of parameters can be changed by hand allowing us to optimize the configuration by observing the corresponding changes to the phase distribution.

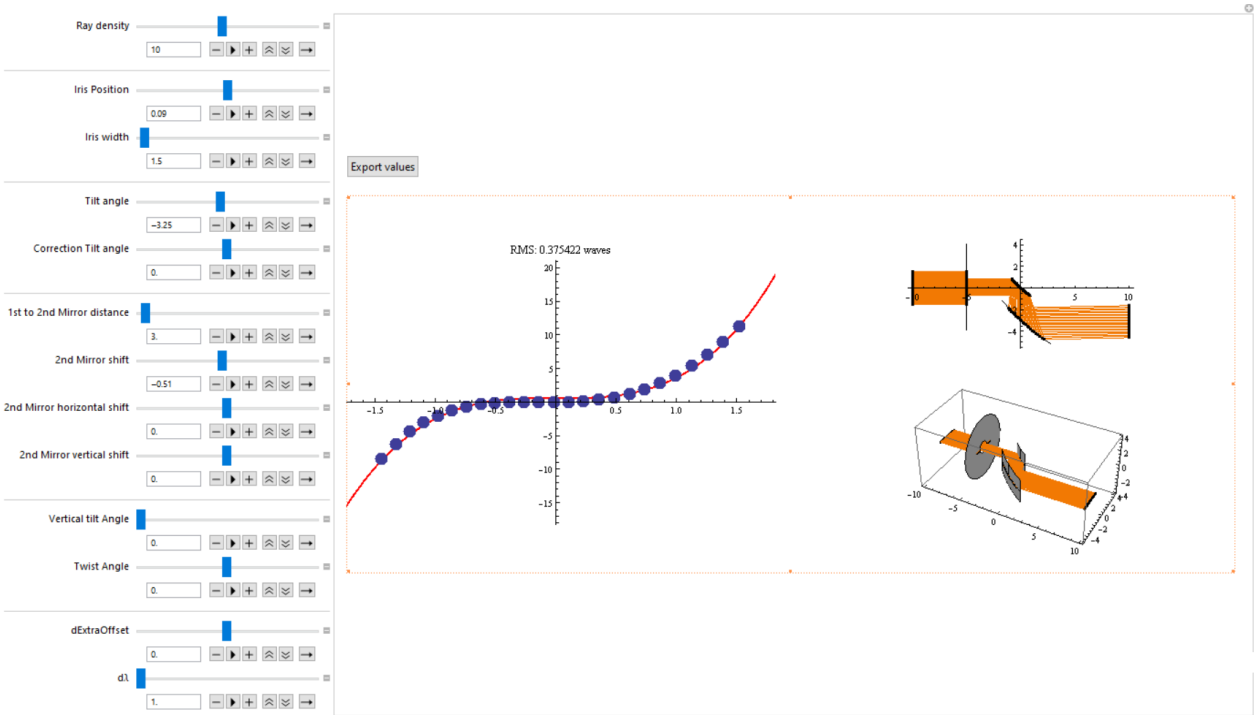


Figure 24

The parameters conserning the rays are the wavelength $\lambda$ and the ray density. The parameters to be changed conserning the geometry are summed up in the following table :

| *Orientation* | *Distance* | *Iris* |
|---|---|---|
| Tilt angle $\theta$ | 1st to 2nd mirror distance $d$ | Iris position |
| Vertical tilt angle $\phi$ | 2nd mirror shift | Iris width |
| Corection tilt angle $\Delta\theta$ | 2nd mirror horizontal shift $\Delta y$ | |
| Twist angle $\psi$ | 2nd mirror vertical shift $\Delta z$ | |

Table 2: Design parameters

*Orientation:* The angles $\theta, \phi$ refer to the angles that define the unit normal to the vertex of each surface as in Eq. (5.1). The angle $\psi$ accounts for any rotation of the optical element around the axis formed by the unit normal to the vertex. The correction tilt angle $\Delta\theta$ is an angle that allows to independently change the orientation of the second optical element as defined in Eq.(5.1).

*Distance:* The first to second mirror distance $d$ is the euclidean distance from the vertex

of the first element to the vertex of the second. The second mirror horizontal, vertical shift $\Delta y, \Delta z$ account for additional, independent displacements of the second mirror.

After setting the parameters the optical path length of each ray is calculated. The corresponding plot is created after centering the phase distribution around zero. Furthermore the user can fit a function of choice on the raytracing data and be aware of the quality of the phase distribution through the *RMS error*. Additionally, the top view and three dimensional image of the optical system allow the user to supervise the optimization process.

At first we show that such an optical system can successfully isolate aberration terms up to 4th order. Following a similar approach to [7]. Using numerical raytracing simulations in *Optica* we perturb the prototype system shown in Fig. 23 and iteratively tune the system's parameters, in order to isolate each of the Taylor series terms in Eq. 4.1. In our simulations we set the initial beam to be an one dimensional line of parallel rays. The optical path each ray travels is then calculated. The graphs that follow depict the spacial phase distribution at the output as a function of ray height $x$ on the image plane. Simulation data (blue points) were also fitted with the corresponding $x^m$ Taylor term to evaluate the efficiency of the process. The *RMS error* from the desired distribution, and the dynamic range are also estimated.

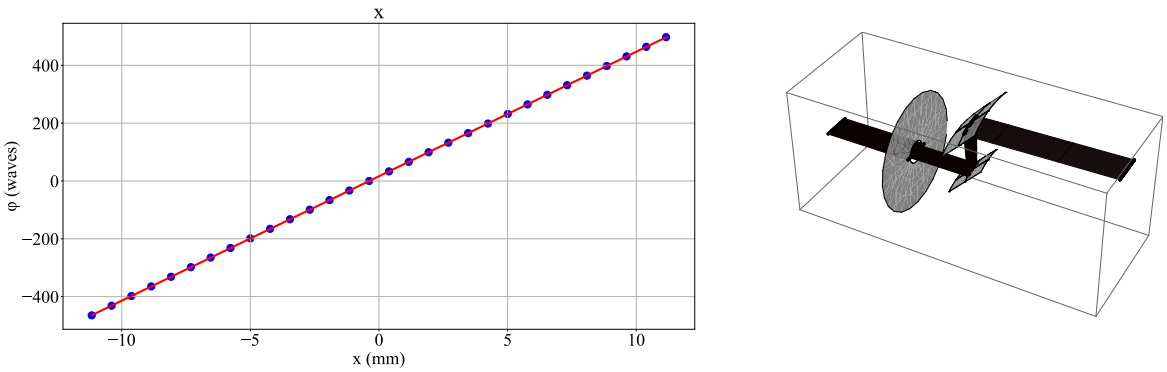


Figure 25: Phase modulator configured for linear phase. (a) Phase distribution in the output (b) 3D representation of the system configuration

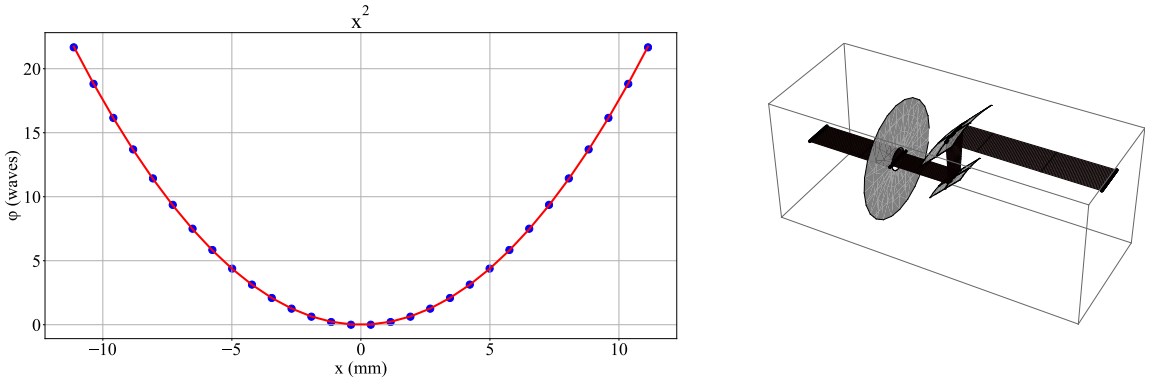


Figure 26: Phase modulator configured for quadratic phase. (a) Phase distribution in the output (b) 3D representation of the system configuration

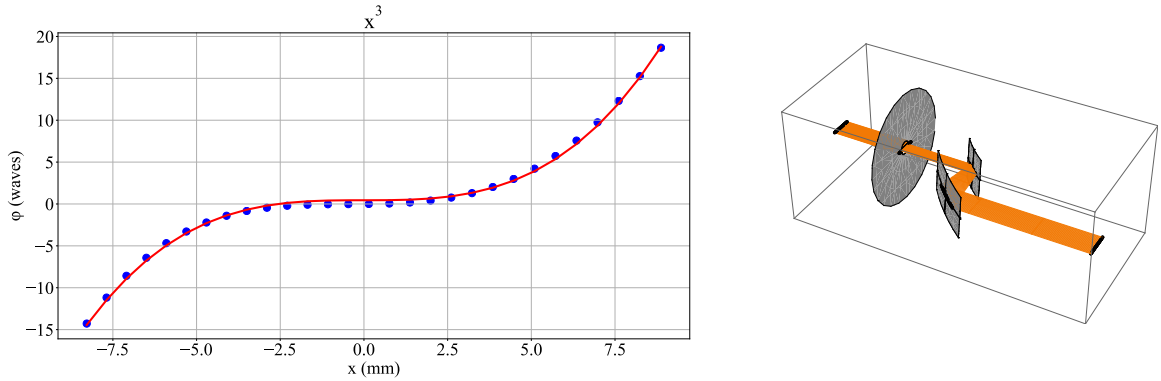


Figure 27: Phase modulator configured for cubic phase. (a) Phase distribution in the output (b) 3D representation of the system configuration

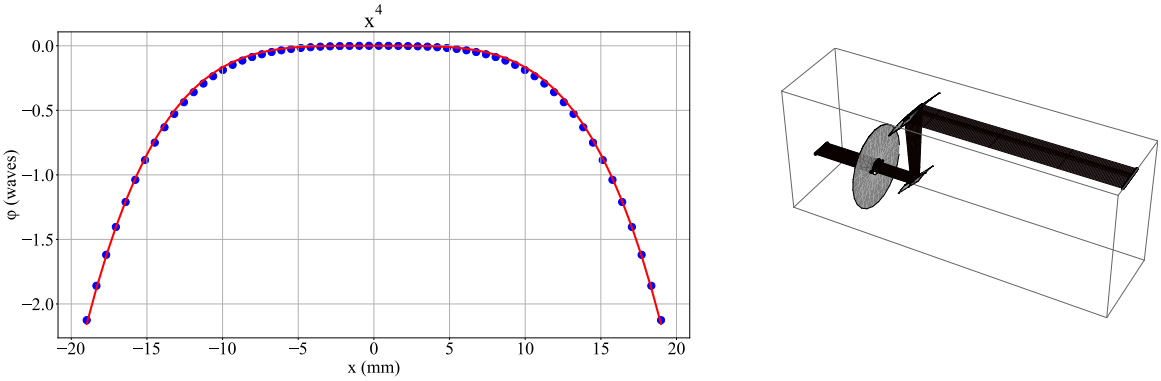


Figure 28: Phase modulator configured for quartic phase. (a) Phase distribution in the output (b) 3D representation of the system configuration

| | $\phi(x)$ | *RMS (waves)* | *Dynamic Range (waves)* | $\lambda$ ($\mu$m) |
|---|---|---|---|---|
| *linear* | $43.047 \cdot x$ | 0.19 | 962 | 0.8 |
| *quadratic* | $0.1755 \cdot x^2$ | 0.027 | 21.7 | 0.8 |
| *cubic* | $0.03 \cdot x^3$ | 0.29 | 33 | 1.0 |
| *quartic* | $-16.6149\ 10^{-6} \cdot x^4$ | 0.016 | 2.12 | 0.8 |

Table 3: Isolation of the Seidel $4^{th}$ order terms.

Since it is possible to modulate the wavefront in such a way so that the Taylor terms are isolated, the next step is to examine if the phase distributions of well known functions can also be reproduced [7]. We advocate that by combining various aberration terms one can approximate any continuous phase distribution around a point using Taylor's theorem.

Up until now by isolating aberration terms, we optimized the configuration so that only one term dominates while the others are minimized. So in order to generate any continuous phase distribution we optimize the optical system so that the coefficients of Eq. (4.1) match

the corresponding Taylor coefficients of the required function. Again with numerical simulations we show that the device can be used as a continuous phase modulator by reproducing some common algebraic functions.

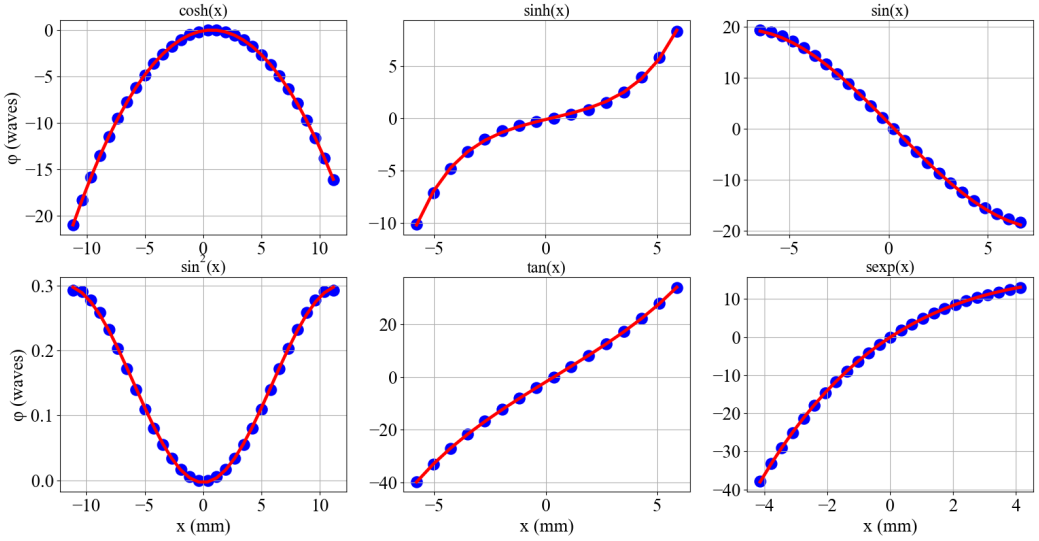


Figure 29: Raytracing results demonstrating that prototype reflecting system can be tailored so that the induced phase modulation can reproduce a variety of functions

| $\phi(x)$ | *RMS (waves)* | *Dynamic Range (waves)* | $\lambda$ ($\mu$m) |
|---|---|---|---|
| $-222.07\cosh(0.03-0.04x)$ | 0.01 | 21.0 | 0.8 |
| $-1.02\sinh(0.11-0.49x)$ | 0.11 | 18.4 | 0.8 |
| $19.56\sin(0.06-0.20x)$ | 0.25 | 37.7 | 0.8 |
| $0.302\sin(7.085\cdot10^{-17}+0.133x)^2$ | 0.002 | 0.3 | 0.8 |
| $-42.298\tan(0.043-0.122x)$ | 0.07 | 73.8 | 0.8 |
| $5.4xe^{-0.1x}$ | 0.1 | 50.8 | 0.8 |

Table 4: Realization of various functions

We conclude that such a device can be used as a continuous phase mask. Any continuous phase distribution can be generated by tuning the system appropriately.

## 5.2 Spectral Bandwidth

The spectral bandwidth of an optical device refers to the wavelength (or frequency) range over which the device complies with specifications. The most important specification parameters for our reflective pahse modulation system are the following:

- The beam quality measured by the *RMS* difference of the resulting phase distribution compared to the required one.
- Dynamic range measured by the phase range ($\Phi_{max} - \Phi_{min}$) achieved by the device at the wavelength of operation.

In contrast to the refractive version of the phase modulator system [8] the reflective version of the system [7] the geometric and the optical path are identical and independent of the wavelength. Denoting the optical path as $L(x)$ the phase distribution $\phi(x, \lambda_0)$ can be calculated as:

$$\phi(x, \lambda_0) = \frac{2\pi}{\lambda_0} L(x)$$

The dynamic range $D_0$ of the phase distribution is then simply calculated as :

$$D_0 = |\phi_{max} - \phi_{min}| = \frac{2\pi}{\lambda_0} |L_{max} - L_{min}|$$

The inverse dependence of $D$ on wavelength practically limits the useful spectral bandwidth. The maximum wavelength of operation is set by the application requirements on the minimum dynamic range the device should achieve.Whereas the shortest wavelength limit is defined by the quality of the phase distribution, here quantified by the *RMS* error, since $\phi(x, \lambda_0)$ also has an inverse dependence on $\lambda$.

To showcase the above we plot the logarithm of the $RMS$ error, dynamic range versus wavelength diagrams for a set up that achieves cubic phase modulation for $\lambda_0 = 1\mu m$.

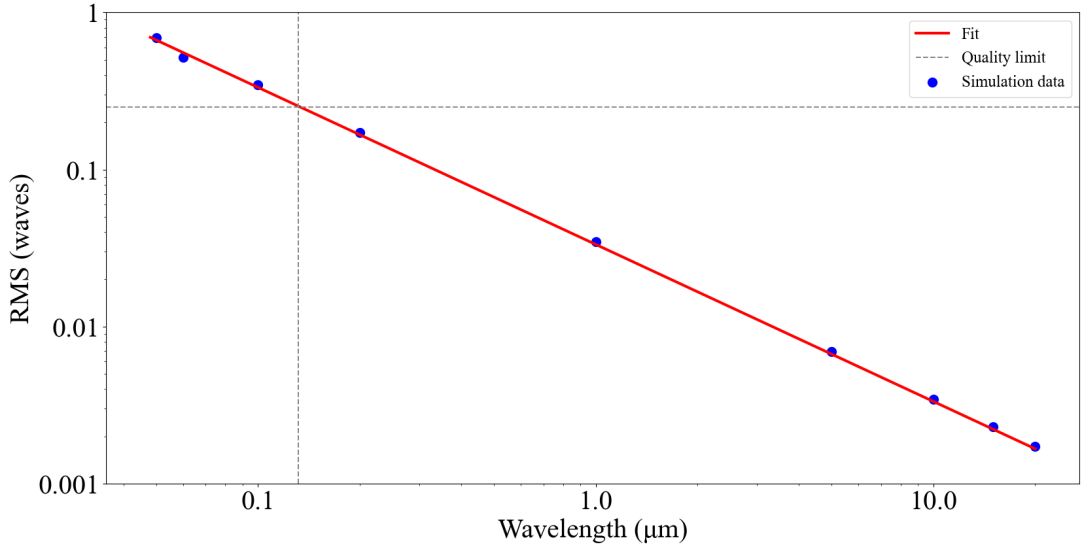


Figure 30: Dependence of *RMS* as a function of the operation wavelength (in Log-Log units)

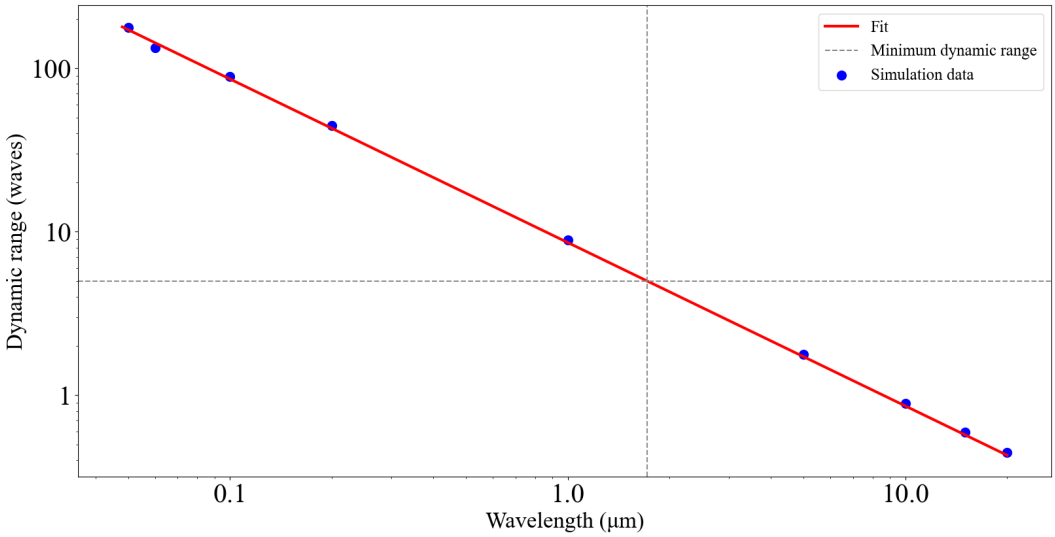


Figure 31: Dependence of Dynamic range $D_0$ as a function of the operation wavelength (in Log-Log units)

| **Fitted Functions of Fig. 30,31** |
|---|
| $RMS(\lambda) = 0.033\ \mu\text{m}/\lambda$ |
| $D(\lambda) = 8.59\ \mu\text{m}/\lambda$ |

A typically used upper limit of the $RMS$ error of an optical system should achieve is $\lambda/4$ [3]:

$$RMS_{max} = \lambda_0/4 = 0.25 \text{ waves} \rightarrow \lambda_{min} = 0.13\mu m$$
$$D_{min} = 5 \text{ waves} \rightarrow \lambda_{max} = 1.72\mu m$$

The useful bandwidth of operation is found to be $\Delta\lambda = 0.72\mu m$. The value for the minimum dynamic range was arbitrarily set to be $5\lambda$. For practical applications a phase distribution with a dynamic range of even one wave is sufficient enough. Taking that into consideration the bandwidth of operation of our device would be even greater by almost an order of magnidude $\Delta\lambda = 8.46\ \mu$m. Additionally since the device consists of reflective mirrors the phase distribution generated is a smooth continuous function in contrast to the phase field generated by a spacial light modulator ($SLM$) where discretization side effects are always present and the bandwidth of operation does not normally exceed $\Delta\lambda = 0.4\mu m$.

## 5.3 Scaling up/down the wavelength of operation

At the previous section it was shown that a configuration achieving cubic phase modulation at a design wavelength $\lambda_0 = 1$ $\mu$m could operate successfully enough in a broad spectral region of $\Delta\lambda = 8.46\mu$m. Due to the limitations posed by the minimum dynamic range, which can not be lower than a wavelength, as well as the quality of the generated phase distribution the spectral bandwidth can not be extended to the far infrared FIR region of say 300 $\mu$m. As a result, one would have to redesign the system so that it is now optimized at a new wavelength of operation $\lambda'$.

A design strategy , instead from redesigning from scratch, is to use scaling. In more detail, for a new wavelength of operation $\lambda^{'} = w\lambda_0$, where $w > 0$ is scaling factor, it is sufficient to use the original design by scaling all distances, mirror physical dimensions, apertures and radii of curvature by the same factor

$$\lambda' = w\lambda_0,\ R_i' = wR_i,\ d_i' = wd_i \tag{5.2}$$

For example, a cubic phase modulation device optimized at $\lambda_0 = 1\mu$m we use the two mirror system depicted below :

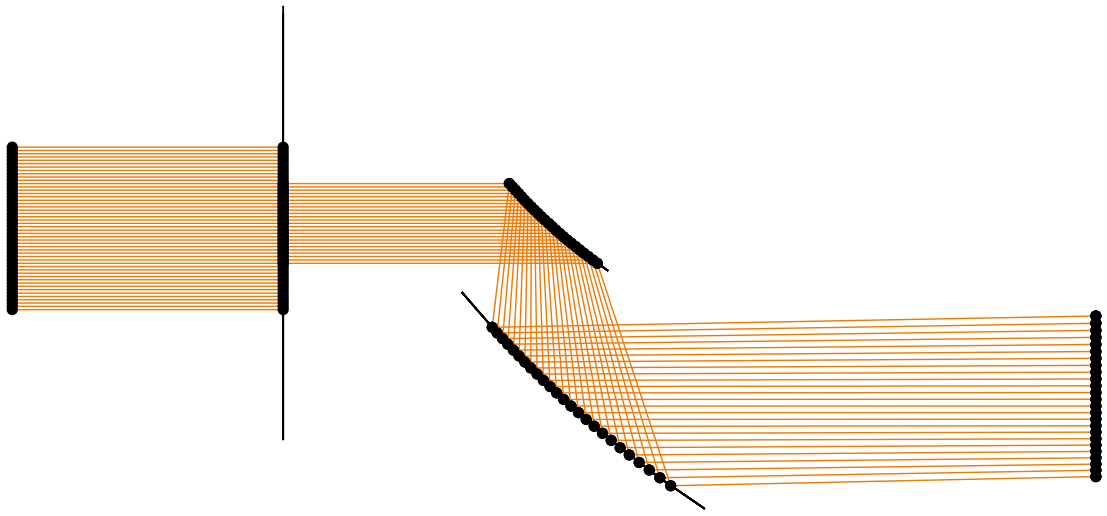

Figure 32: Configuration optimized at $\lambda_0 = 1\mu$m achieving cubic phase modulation.

| | $R_i$ (mm) | **Mirror dimensions** (mm) |
|---|---|---|
| **1st** | 10 | $(2.5 \times 3)$ |
| **2nd** | 20 | $(6 \times 3)$ |

Table 5: Design parameters of the cubic phase modulator

By varying $\lambda$ and scaling the set up accordingly we acquire the phase distribution for each wavelength and plot it in the diagram below.

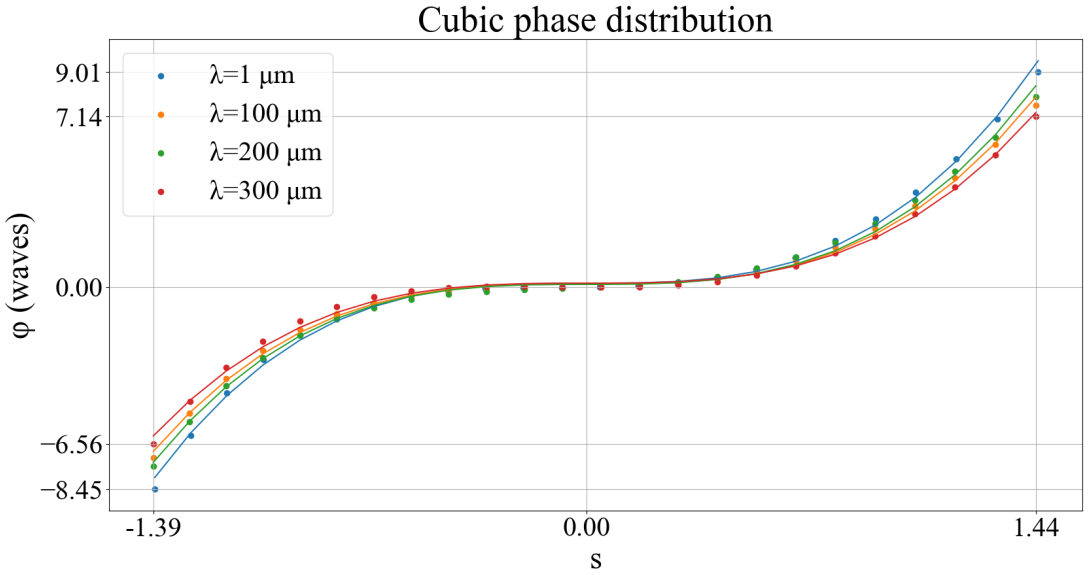


Figure 33: Phase distribution as a function of the normalized coordinate on the exit pupil $s = x/w$, for various scaling parameters $w$.

| **Scale factor** *(waves)* | **Dynamic range** *(waves)* | **RMS** *(waves)* |
|---|---|---|
| 1 | 17.45 | 0.199 |
| 100 | 14.71 | 0.150 |
| 200 | 15.43 | 0.200 |
| 300 | 13.70 | 0.150 |

Table 6: Specifications of scaled systems

It is worth mentioning that the results are presented as a function of the normalized coordinate $s$. We can see that the output field size is directly proportional to the scaling factor $w$. This behaviour is due to mirror apertures that scale with the same factor. It is easy to observe that even at the far infrared region of 300 $\mu$m both the dynamic range and the *RMS* error of the phase distribution have a very small deviation from their initial values. Any differences result from minute imperfections during the initial configuration optimization (at $\lambda_0$ wavelength). These small deviations from a perfect phase distribution (cubic in this case), blow up as the dimensions of the system are scaled accordingly. As a result minor adjustments to the configuration were necessary. The main drawback of such an approach is that since the dimensions of the system scale according to the new operation wavelength, the mirror apertures and the total length of the system grow up in proportion rendering such a device impractical for the far infrared region.

## 5.4 Use of optical system cascading

As discussed in the previous section, where operation at a new wavelength $\lambda = 300\mu$m is designed, to produce an acceptable dynamic range the system mirror apertures are proportionally increased. An alternative approach is to "amplify" the output of of the device by

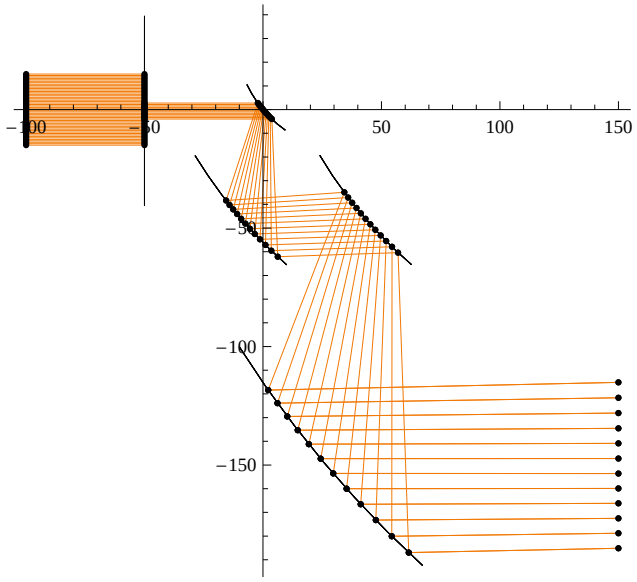


Figure 34: Raytracing of a cascade of two reflective phase modulators that introduces a net cubic phase modulation. Distances are measured in *mm*.

cascading similar devices so that the output of the first is used as an input for the second. In more detail, we investigate how the second device would further modulate the wavefront so that the phase distribution is still functionally the same (cubic in our example) while the dynamic range is increased.

Below we present a cascade of two reflective phase modulators comprised by four mirrors, that introduces a net cubic phase modulation at $\lambda = 300$ $\mu$m.

As we can see in Fig. 34 and Table 7, the radii of curvature of the third and fourth mirror are larger compared to those of the first and second mirror, with the fourth mirror's being the largest. This ensures that the output wavefront will not be heavily aberrated so that one can focus on optimizing the set up by only making adjustments to the orientation of the optical elements as well as the distance separating them. Specifically in the system depicted in Fig. 34 only the distance between the mirrors of each sub-system was tuned. Below we plot the phase distribution of both the two and four mirror system for comparison.

| Mirror | $R_i$ (mm) | **Mirror dimensions** (mm) |
|---|---|---|
| **1st** | 50 | $(25 \times 30)$ |
| **2nd** | 200 | $(60 \times 30)$ |
| **3rd** | 186 | $(60 \times 30)$ |
| **4th** | 452 | $(120 \times 40)$ |

Table 7: Mirror specifications for the system cascade of Fig. 34

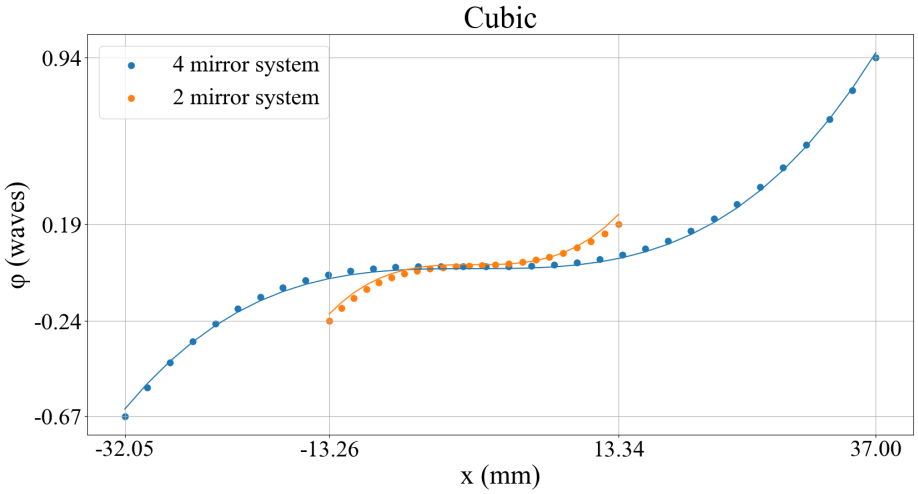


Figure 35: Raytracing results for the phase distribution in the exit of a reflective phase modulator (2 mirror) and a cascade of two reflective phase modulator devices (4 mirror)

| **System** | **Dynamic Range (waves)** | **RMS (waves)** |
|---|---|---|
| 4 Mirror | 1.61 | 0.018 |
| 2 Mirror | 0.43 | 0.006 |

Table 8: Specifications of the 2 and 4 mirror systems

As we can see from Fig. 35 with the cascaded system we achieve a quadrupling of the dynamic range compared to the simple two mirror system. As we demonstrate by cascading two cylindrical beam expanders the dynamic range at $\lambda_0 = 300$ $\mu$m is considerably extended, reaching the the minimum requirement of one wave ($\lambda$).

# 6 Analytic raytracing calculations

In order to better understand the behaviour the reflective phase modulator device, an in-depth mathematical analysis is required. Using the methodology described bellow we have performed a rigorous raytracing analysis. Our goal is to obtain a mathematical expression for the optical path length of a ray as a function of system parameters. Although the optical elements span in 3 dimensions their cylindrical nature allow us to simplify the analysis to two dimensions. In our analysis we consider that the system consists of two cylindrical reflective surfaces $S_1$, $S_2$ and a screen $S_3$ as shown in Fig. 36. The radii of curvature are respectively $r_1, r_2$. Note that the two surfaces do not share the same center.

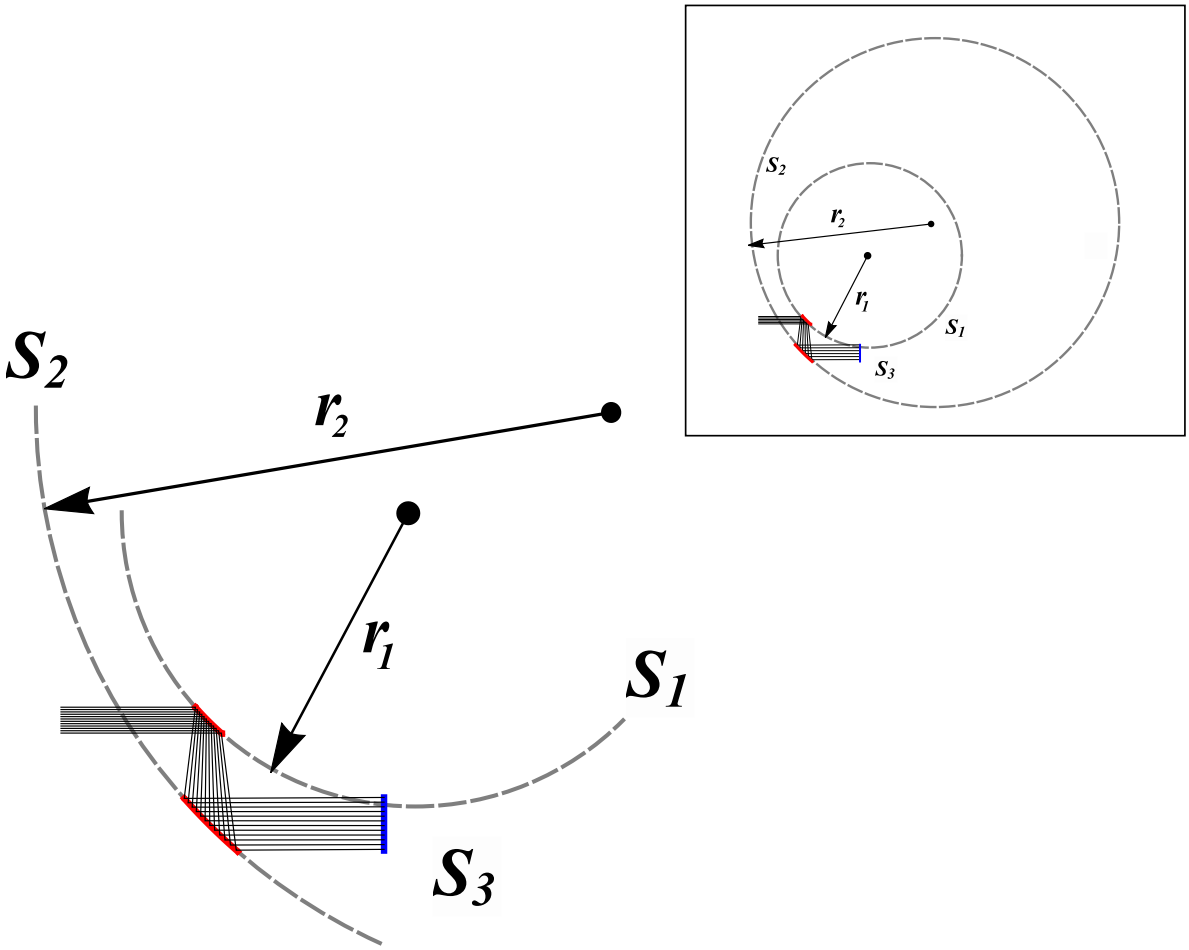


Figure 36: Graphical representation of the geometry of the two reflective spherical surfaces that comprise the phase modulator device. Dashed lines represent the cylindrical surfaces. Actual mirrors are denoted with thick red lines *Inset:* representation of the full geometry

## 6.1 Raytracing

Let's now describe in detail the raytracing steps that we followed in to analytically describe the propagation of a ray through the reflective phase modulator device.

- The ray's starting position and direction are described by $\mathbf{p}_i$ and $\hat{\mathbf{a}}_i$ respectively.
- The intersection point of the ray with a reflective surface described as $\mathbf{p}_{i+1}$ is then calculated.
- The normal to the surface $(S_i)$, at the intersection point, $\hat{\mathbf{n}}_{i+1}$ is then calculated.
- Using the law of reflection the reflected ray's direction $\hat{\mathbf{a}}_{i+1}$ is then estimated.

The process can be repeated for any number of surfaces. In our case, the system consists of two reflective surfaces so two iterations are necessary.

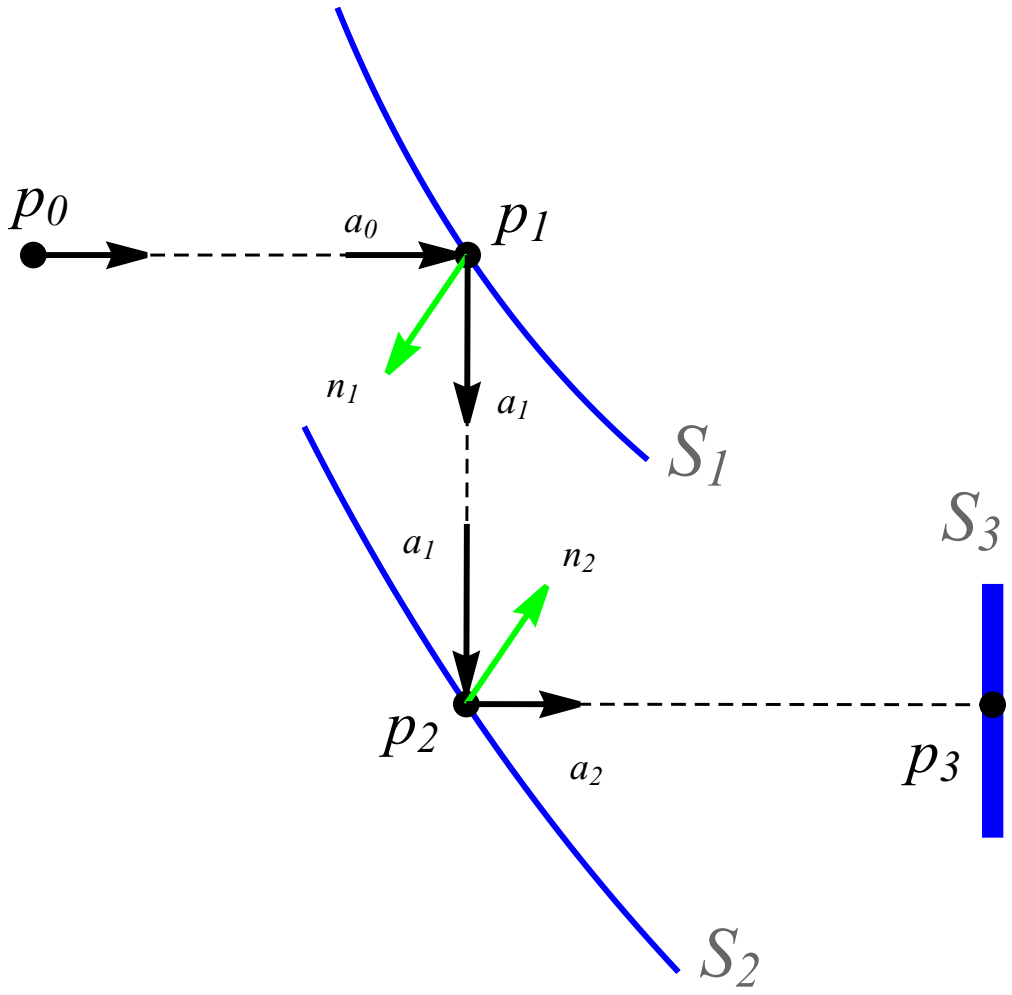


Figure 37: Schematic representation of the reflective system with all raytracing parameters depicted. $\mathbf{p}_i$: intersection points, $\hat{\mathbf{a}}_i$: unitary ray direction vectors, $\hat{\mathbf{n}}_i$ surface normals.

### 6.1.1 Estimation of the intersection of a ray with a circular surface

Assuming a ray with starting position $\mathbf{p}_i$, final position $\mathbf{p}_{i+1}$ and direction $\hat{\mathbf{a}}_i$ the corresponding line equation is :

$$\mathbf{p}_{i+1} = \mathbf{p}_i + \hat{\mathbf{a}}_i d_i$$

where $d_i$ is the distance between $\mathbf{p}_i$ and $\mathbf{p}_{i+1}$.

Assuming that the center of the circular reflective surface $S_{i+1}$, of radius $r_{i+1}$, is described by the position vector $\mathbf{c}_{i+1}$ then the intersection point of that ray with surface can be calculated as follows :
A point $P$ on the circle satisfies the relation

$$\|P - \mathbf{c}_{i+1}\| = r_{i+1}$$

Substituting $P$ with a point on the ray $P \rightarrow \mathbf{p}_i + \hat{\mathbf{a}}_i d_i$ results in a quadratic equation in $d_i$

$$\alpha d_i^2 + \beta d_i + \gamma = 0$$

with

$$\alpha = (\hat{\mathbf{a}}_i \cdot \hat{\mathbf{a}}_i),\ \beta = 2\hat{\mathbf{a}}_i \cdot (\mathbf{p}_i - \mathbf{c}_{i+1})$$
$$\gamma = (\mathbf{p}_i - \mathbf{c}_{i+1}) \cdot (\mathbf{p}_i - \mathbf{c}_{i+1}) - r_{i+1}^2$$

Solving for $d_i$ we have :

$$d_i = \frac{-\beta \pm \sqrt{\beta^2 - 4\alpha\gamma}}{2\alpha} \tag{6.1}$$

Depending on the value of the discriminant $\Delta = \beta^2 - 4\alpha\gamma$ there may be two, one or no intersections of the ray and the surface. Assuming that the ray does intersect with the reflective surface, only one of the solutions is physically correct and may be taken into account.

Substituting $d_i$ back in the line equation will give us the intersection point $\mathbf{p}_{i+1}$. Since both $\mathbf{p}_i$ and $\hat{\mathbf{a}}_i$ are functions of the ray coordinates, $d_i$ will also be a function of coordinates and system parameters $(\mathbf{c}_{i+1}, \mathbf{r}_{i+1})$ .

### 6.1.2 Ray intersection with a plane (observation screen)

If $\mathbf{c}_{i+1}$ is an arbitrary point on the plane of the screen and $\hat{\mathbf{n}}_{i+1}$ is the normal to the plain, a generic point $P$ on that surface satisfies :

$$(P - \mathbf{c}_{i+1}) \cdot \hat{\mathbf{n}}_{i+1} = 0$$

Substituting $P$ with a point on the ray and solving for $d_i$ we get:

$$d_i = -\frac{(\mathbf{p}_i - \mathbf{c}_{i+1}) \cdot \hat{\mathbf{n}}_{i+1}}{\hat{\mathbf{a}}_i \cdot \hat{\mathbf{n}}_{i+1}} = \|\mathbf{p}_{i+1-\mathbf{p}_i}\| \tag{6.2}$$

### 6.1.3 Reflection from a cylindrical surface

Once the intersection point is calculated, the normal to the surface $\hat{\mathbf{n}}_{i+1}$ at that point can be found and by using the law of reflection the reflected ray's direction can be then estimated:

$$\hat{\mathbf{a}}_{i+1} = \hat{\mathbf{a}}_i - 2(\hat{\mathbf{a}}_i \cdot \hat{\mathbf{n}}_{i+1}) \cdot \hat{\mathbf{n}}_{i+1} \tag{6.3}$$

The surface normal can be calculated in a number of ways depending on representation.Bellow $r$ is the radius, $c_x, c_y$ are the coordinates of the centre of the surface and $\hat{\mathbf{n}}$ is the normal to the surface.

- Using an implicit representation of the circle :

$$F(x, y) = (x - c_x)^2 + (y - c_y)^2 - r^2 = 0$$

$$\hat{\mathbf{n}} = \frac{\nabla F}{\|\nabla F\|}$$

- Using a parametric representation of the circle :

$$S = [c_x + rcos(\theta), c_y + rsin(\theta)], \theta \in [0, 2\pi]$$

$$\hat{\mathbf{n}} = \frac{S_{\theta\theta}}{\|S_{\theta\theta}\|}$$

- Using rational parametrization of the circle [1]:

$$S = \Big[c_x + r\Big(\frac{m^2-1}{m^2+1}\Big), c_y + r\Big(\frac{-2m}{m^2+1}\Big)\Big],\ m \in [-\infty, +\infty]$$

$$\hat{\mathbf{n}} = \frac{S_{mm}}{\|S_{mm}\|}$$

  where $S_{\theta\theta}$ and $S_{mm}$ denote the second partial derivative with respect to $\theta$ , $m$.

*Rational parametrization of the circle:*

Let's describe in more detail the rational parametrization of the circle, a parametrization approach that is not so commonly used. To simplify our analysis we assume that the center of the circle is at the coordinate system origin so $c_x = c_y = 0$ and that $r = 1$ (unitary radius). Under these assumptions the parametric equation of a circle takes the form:

$$S(m) = \Big[\frac{m^2-1}{m^2+1}, \frac{-2m}{m^2+1}\Big]$$

At first it is easy to observe that $S_x^2 + S_y^2 = 1$. Also $S_x(m)$ is an even function whereas $S_y(m)$ is odd. As a result two points on the circle with the same absolute value of the parameter $m$ will be symmetric with respect to the horizontal axis. So as $m$ takes values symmetrically around 0, $S(m)$ traces an arc of the curve which is symmetric with respect to the horizontal axis. In this representation, the last point namely $S(\pm\infty)$ is excluded but can be found, by taking the limits for $S_x(m)$ and $S_y(m)$ at $\pm\infty$, to be 1 and 0 respectively. Below we plot $S(m)$ for $m \in [-2, 2]$: As we will demonstrate such a parametrization, although in principle more complex, allows us to define in a more closed form the optical path length of

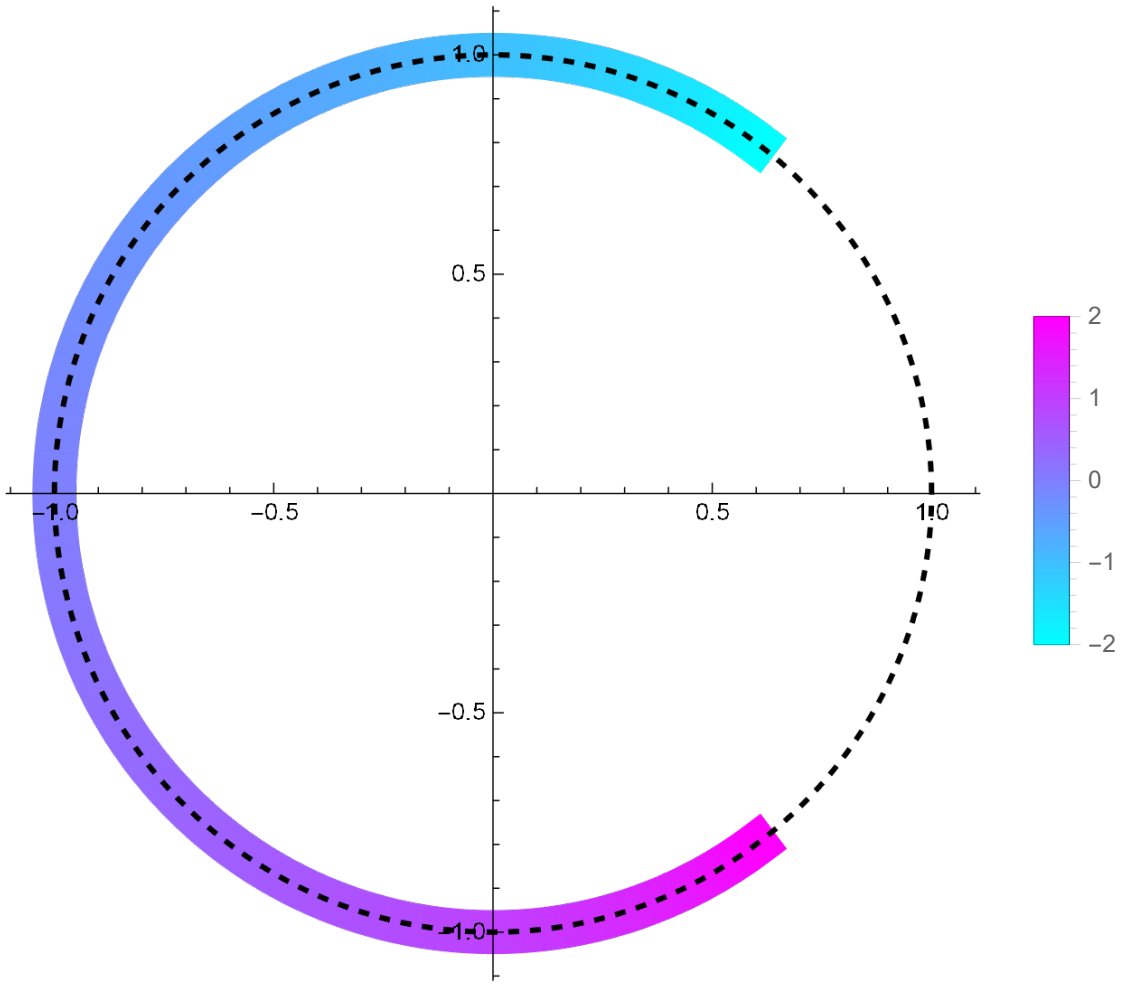


Figure 38: Rational parametrization of the circle. The colors indicates the corresponding $m$ values.

a ray through our system. Also since only the second and third quadrant of the cylindrical reflective surfaces are used in our system as shown in Fig. 36 the values for $m$ are restricted in the range of $[-1, 1]$, simplifying the evaluation process of any expression depending on that variable. Finally, this parametrization provides an alternative way to describe the quantities of interest without the use of trigonometric functions, making algebraic expressions easier to manipulate.

## 6.2 Estimation of the optical path length

The optical path length $d$ of a ray that propagates through the system is the sum of three separate paths:

- the distance $d_1$ travelled from the starting plane to the first mirror.
- the distance $d_2$ $1^{st}$ to the $2^{nd}$ mirror.
- the distance $d_3$ travelled from the $2^{nd}$ mirror to the observation screen.

Since we define all rays to start from the same input plane the initial points lie on a line $p_0 = [p_{0x}, y]$. Likewise, all rays are parallel to each other $a_0 = [1, 0]$ so we can easily describe the first line segment as a function of $\theta$ Fig. 39.

$$d_1 = (c_{1x} - p_{0x}) - |r_1 cos(\theta)| \tag{6.4}$$

Making use of the notation described above as well as the parametric equation for the circle $S(\theta)$ we will find the intersection point with the second surface $S_2$. Assuming that all rays intersect the $1^{st}$ circular reflective surface, the intersection points will be of the form :

$$\mathbf{p_1} = [c_{1x} + r_1 cos(\theta), c_{1y} + r_1 sin(\theta)]$$

where $\theta$ varies within an appropriate range in order to trace the illuminated cylindrical mirror surface . The normal to the surface can then be found to be :

$$\hat{\mathbf{n}}_1 = [cos(\theta), sin(\theta)]$$

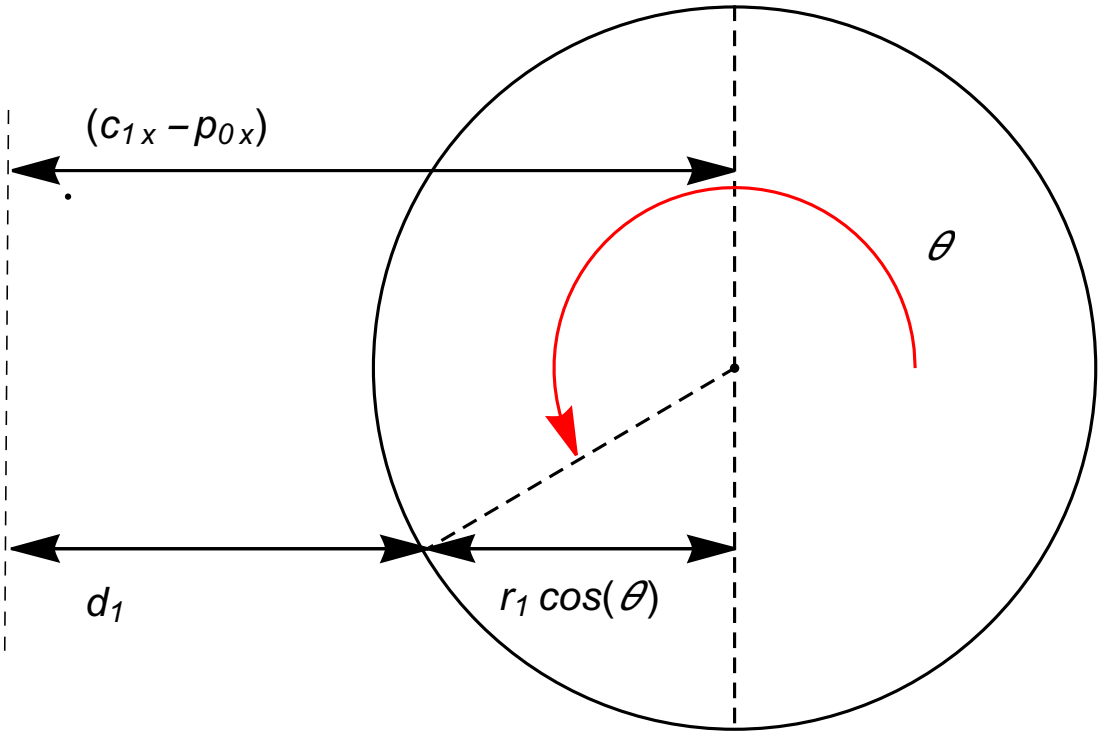


Figure 39: Estimation of the $1^{st}$ distance $d_1$.

using the law of reflection Eq. (6.3) and $\hat{\mathbf{a}}_0 = [1, 0]$ we can find the direction of the reflected ray:

$$\hat{\mathbf{a}}_1 = [-cos(2\theta), -sin(2\theta)]$$

We now have all the necessary information to find $d_2$ through Eq. (6.1). In more detail we have:

$$d_2 = \frac{1}{2}(2r_1\cos(\theta) - 2\cos(2\theta)\delta_x - 2\sin(2\theta)\delta_y)) + \sqrt{-4r_1^2\sin^2(\theta) + 8r_1\sin(\theta)\left(\sin(2\theta)\delta_x - \cos(2\theta)\delta_y\right) + 4r_2^2 - 4\left(\cos(2\theta)\delta_x - \sin(2\theta)\delta_y\right)^2} \tag{6.5}$$

where $\delta_x = c_{2x} - c_{1x},\ \delta_y = c_{2y} - c_{1y}$. Using the above, we find the second intersection point:

$$\mathbf{p}_2(\theta, \mathbf{c}_i, r_i) = \mathbf{p}_1(\theta, \mathbf{c}_i, r_i) + \hat{\mathbf{a}}_1(\theta)d_2$$

Since we have analytically estimated $\mathbf{p}_2(\theta, \mathbf{c}_i, r_i)$ and $\hat{\mathbf{a}}_1(\theta)$ we only need now to estimate $\hat{\mathbf{n}}_2$ in order to get the direction $\hat{\mathbf{a}}_2$ after the second reflection. Assuming that the ray intersects $S_2$ at some arbitrary point the normal vector at that point will be:

$$\hat{\mathbf{n}}_2 = [cos(\phi), sin(\phi)]$$

where $\phi$ is an angular parameter which allows us to describe $S_2$. We can eliminate the new parameter, so the problem only depends on one variable, making use of the expression for $\mathbf{p}_2(\theta, \mathbf{c}_i, r_i)$. In more detail we have :

$$\mathbf{p_2} = [c_{2x} + r_2\cos\phi,\ \ c_{2y} + r_2\sin\phi] = [p_{2x}(\theta), p_{2y}(\theta)]$$

$$\Rightarrow \cos\phi = \frac{p_{2x}(\theta) - c_{2x}}{r_2},\ \ \sin\phi = \frac{p_{2y}(\theta) - c_{2y}}{r_2} \tag{6.6}$$

Substituting the expression for the normal vector we can find $\hat{\mathbf{n}}_2$ as a function of $\theta$ (see Appendix). Using the law of reflection we can find the new direction vector $\hat{\mathbf{a}}_2(\theta, \mathbf{c}_i, r_i)$. The next step is to calculate the distance $d_3(\theta, \mathbf{c}_i, r_i)$ from $S_2$ to $S_3$ through Eq. (6.2). Thus, we have estimated all the necessary information to calculate the intersection point of a ray with the screen.

$$\mathbf{p}_3(\theta, \mathbf{c}_i, r_i) = \mathbf{p}_2(\theta, \mathbf{c}_i, r_i) + \hat{\mathbf{a}}_2(\theta)d_3$$

The analytic estimation of $d_3(\theta, \mathbf{c_i}, r_i)$ and $p_{3y}(\theta, \mathbf{c_i}, r_i)$ is quite extended for this section and is given in detail in the Appendix.

## 6.3 Approximations

In the previous sections we have analytically estimated the total optical path length $d$ as a function of system parameters and a free parameter $\theta$. It is important to mention that $\theta$ serves as an alternative to the input ray coordinates. As our interest lies the modulation of the phase distribution when the system parameters are changed, it is desirable to express the total optical path $d$ as a function of the ray coordinates in the output. To elaborate, we have already seen that the various aberration terms can be properly combined so that the phase distribution resembles a Taylor expansion of known functions. So if $y_s$ is the ray height coordinate on the output screen we can write:

$$d(y_s, \mathbf{c_i}, r_i) = \sum_{i=0}^{k} a_i (y_s)^i = a_0 + a_1 y_s + a_2 y_s^2 + a_3 y_s^3 + ... + a_m y_s^k \tag{6.7}$$

In this description, the coefficients of the Taylor expansion of the optical path length depend on the system parameters. Consequently, the optimization of an optical system so that it achieves a required phase distribution reduces down to finding the appropriate system parameters so that the respective coefficients satisfy its Taylor expansion. Inversely, this approach can help us identify the system configurations that would achieve such a task.

In our case :

$$d = d_1 + d_2 + d_3 = f(y_s, \mathbf{c}_i, r_i)$$

where $y_s \equiv p_{3y}(\theta, \mathbf{c}_i, r_i)$ (output screen).

At first we have to estimate the analytic functional relation between the input and output coordinates. Unfortunately, the output $p_{3y}$ is a non-invertible function of the input $\theta$. To bypass this problem we use an approximation of the output coordinates. In more detail, we expand $y_s$ around an arbitrary point and keep terms up to $1^{st}$ order. At this point it is convenient to change the parametrization of the problem because trigonometric functions such as $\cos\theta,\ \sin\theta$ are hard to work with, considering that derivatives of very long expressions are involved in our series expansion. Making the direct substitutions:

$$cos(\theta) = \frac{-1 + m^2}{1 + m^2}, sin(\theta) = \frac{-2m}{1 + m^2}$$

all quantities so far can be expressed as a function of $m$. So up to first order the output becomes :

$$y_s = A + B(m - m_0)$$

where $A = y_s(m)|_{m=m_0}$ , $B = \frac{\partial y_s}{\partial m}|_{m=m_0}$ and $m_0$ is an arbitrary point around which we expand. Inverting the above linear dependence we get :

$$m = (y_s - A)/B + m_0$$

It is worth noting that when $m = m_0$ , $y_s = A$. So making a coordinate shift $y_s^{'} = y_s - A$ we get:

$$m = y_s^{'}/B + m_0$$

Now we can substitute this expression in $d(m)$ and describe the optical path length as a function of the output $d(y'_s, \mathbf{c}_i, r_i, m_0)$ and also estimate the Taylor coefficients up to $4^{th}$ order:

$$a_k(\mathbf{c_i}, r_i, m_0) = \frac{d^k(0)}{k!},\ k = 0, 1, \ldots, 4$$

At this point it is necessary to explain , in more detail, the importance of the new parameter $m_0$ that was introduced when a linear relationship between input and output coordinates was established.

In an ideal beam expander, where parallel incidence is assumed the output rays will be displaced by an equal amount $\Delta y = y_s - y_{in}$ while preserving their orientation. In our case since the reflective elements are curved surfaces the direction vectors inevitably become functions of the ray position and the system parameters. As a result each ray is displaced by a different amount which depends on the ray's initial position $y_{in}$ and the system parameters.

Without loss of generality the input ray parameters can be parametrized using a new variable, in our case $m$. So the ray displacement take the form $\Delta y \to \Delta y(\mathbf{c}_i, r_i, m)$. Provided that $\Delta y$ is a continuous, differentiable, function of $m$ we can write :

$$\Delta y \approx \Delta y(m_0) + \frac{1}{2}\Delta' y(m_0)(m - m_0) + \mathcal{O}(2) \tag{6.8}$$

From the above equation it is clear that the total ray displacement can be described as a sum of a fixed amount $\Delta y(m_0)$ (as in the case of a perfect beam expander) plus an additional one, that depends on the partial derivatives, accounting for the displacement caused by the different directions rays with slightly different origins have when they reach the screen. It is clear now that $m_0$ serves as the parameter that marks a chief ray whose displacement is considered fixed for all rays and the exact reason why the coordinate shift $y'_s = y_s - A$ allows us to expand around zero.

In order to check the validity of our approximation we first optimize configurations using numerical raytracing software *(Optica)* and achieve linear, quadratic, cubic phase distributions. Then we extract the system parameters $\mathbf{c}_i, r_i$ and the iris position $y_{iris}$ and width $w$. The last two parameters allow us to determine the appropriate range of values the free parameter $m$ takes. If $y_t, y_b$ are the positions of the top and bottom ray then

$$y_t = y_{iris} + w/2$$
$$y_b = y_{iris} - w/2$$

For parallel incidence on the first circular surface $S_1$ we can use the rational parametrization to find the values that $m$ takes for those two rays.

$$c_{1y} + r1\Big(\frac{-2m}{1+m^2}\Big) = y_{t,b}$$

Solving the quadratic in $m$ and obtaining the solution that matches the numerical raytracing we can find the values for $m$ of the top and bottom ray, namely $m_{t,b}$. For the systems considered here the second and third quadrant is used. There the parametrization is set up so those quadrans lie in the interval $[-1, 1]$ for the $m$ parameter so we can easily identify the right value. The free parameter $m_0$ will lie in the interval $[m_t, m_b]$ and for the sake of simplicity we take $m_0$ to be the midpoint of the interval. Now all the necessary quantities for our approximation namely $\mathbf{c}_i, r_i, m_0$ are known and by direct substitution we can plot the results of the approximation along with the full analytic expression and raytracing data for comparison bellow.

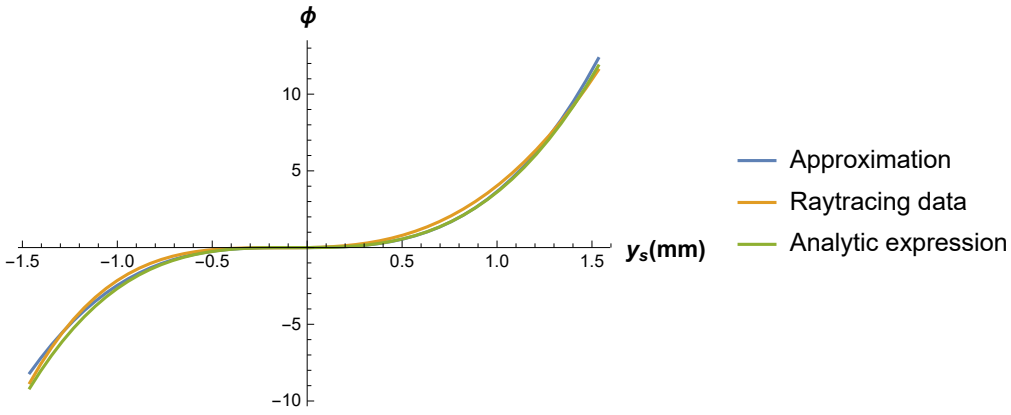


Figure 40: Comparison between raytracing results, the analytic expression and the series expansion of the phase distribution for a configuration that achieves cubic phase distribution.

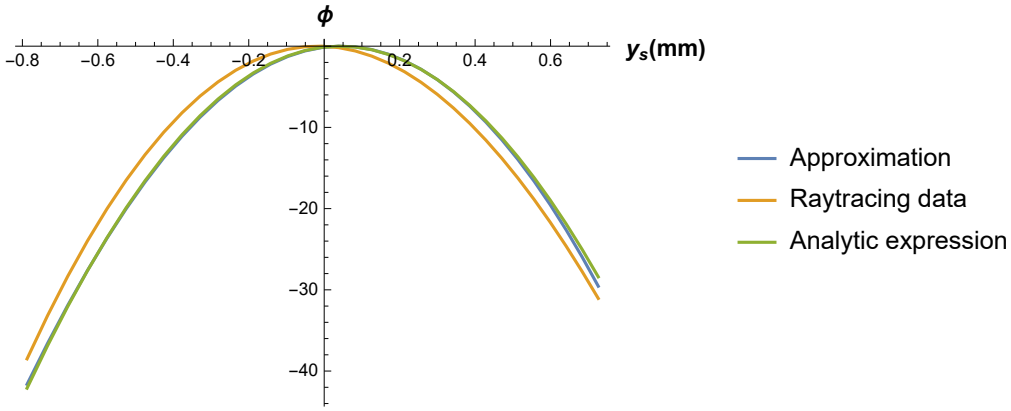


Figure 41: Comparison between raytracing results, the analytic expression and the series expansion of the phase distribution for a configuration that achieves quadratic phase distribution.

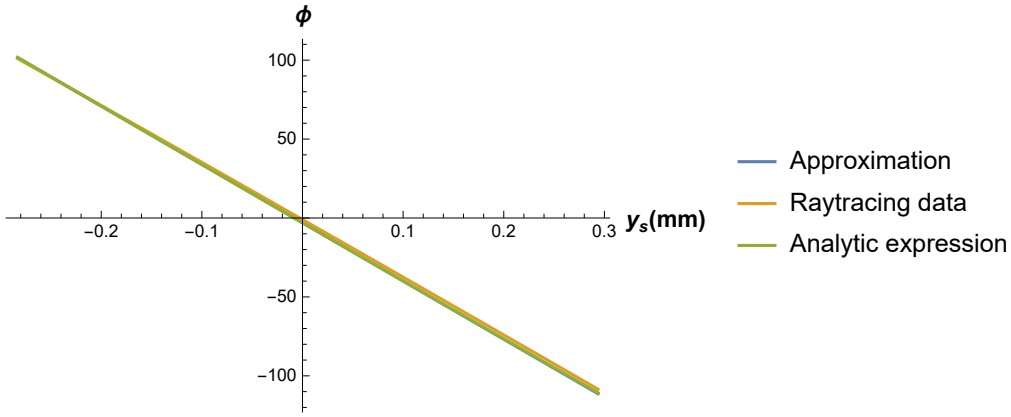


Figure 42: Comparison between raytracing results, the analytic expression and the series expansion of the phase distribution for a configuration that achieves clinear phase distribution.

# Conclusions

In this thesis we have studied the properties of a prototype phase modulation system consisting of two cylindrical mirrors that uses aberrations to achieve a continuous modulation of the phase distribution in the output. In our study, we firstly confirmed, using numerical raytracing simulations that by varying the distance and orientation of the elements of the system one can isolate specific aberration terms. Furthermore, we shown that the Seidel aberrations, can be represented as up to the $4^{th}$ order terms of a Taylor series expansion of any continuous phase distribution. Using this analogy, we have demonstrated that various continuous phase distributions can be reproduced by perturbing the device configuration. Likewise, this study was focused on design strategies that will allow us to extend the phase modulation device operation to a much broader spectral range. We have shown, using a scenario of cubic phase modulation as our reference, that the device is scalable with regard to the wavelength of operation, to a range that extends to THz frequencies. Besides direct scaling up approaches that blow up the system's physical dimensions, we have also studied alternative approaches like system cascading stacking configurations. Furthermore, we have performed a rigorous, analytic raytracing analysis of the optical system. In our analysis the analytic formulas of the optical path length ($OPL$) traveled by rays, as they propagate through the system, was retrieved. Using approximations we have retrieved an analytic description of the ($OPL$) as a series expansion of the ray output height. Our analytical results agree well with numerical raytracing. Although quite long and complex our analytic results provide a systematic approach to optimize of the system configuration in order to achieve a required phase modulation.

# Appendix

Here we present in detail the derivation of the the relations presented in of Ch. 6.2.
At first lets start with Eq. (6.6):

$$
\begin{aligned}
cos(\phi) = \\
&\frac{1}{2r_2}\Big\{4r_1\cos\theta\sin^2\theta - 2\sin^2(2\theta)\delta_x + \sin(4\theta)\delta_y \\
&\quad - \cos(2\theta)\Big[2r_1^2\cos(2\theta) \\
&\qquad + 4\delta_x\left(4r_1\sin^2(\theta)\cos(\theta) + \delta_y(\sin(4\theta)+\cos(4\theta))\right) \\
&\qquad + 4r_1(\sin\theta - \sin(3\theta))\delta_y \\
&\qquad - 2r_1^2 + 4r_2^2 - 4\cos^2(2\theta)\delta_x^2 - 4\cos^2(2\theta)\delta_y^2\Big]^{\frac{1}{2}}\Big\}
\end{aligned}
$$

$$
\begin{aligned}
sin(\phi) = \\
&\frac{1}{2r_2}\Big(-\delta_y(1+\cos(4\theta)) + r_1(\sin\theta - \sin(3\theta)) + \sin(4\theta)\delta_x - \sin(2\theta)\Big[2r_1^2\cos(2\theta) + \\
&4\delta_x\left(4r_1\sin^2(\theta)\cos(\theta) + \delta_y(\sin(4\theta)+\cos(4\theta))\right) + 4r_1(\sin\theta - \sin(3\theta))\delta_y - 2r_1^2 + \\
&4r_2^2 - 4\cos^2(2\theta)\delta_x^2 - 4\cos^2(2\theta)\delta_y^2\Big]^{\frac{1}{2}}\Big)
\end{aligned}
$$

where $\delta_x = c_{x2} - c_{x1}$ and $\delta_y = c_{y2} - c_{y1}$.

Those two relationships provide a way to eliminate the parameter $\phi$ that appears after the second reflection from $S_2$. We do so by first calculating all quantities related to the second surface as functions of two variables $(\theta, \phi)$ and then directly substituting the above relations.

The relation for the opl from $S_2$ to $S_3$ is given by:

$$d_3(\theta,\phi) = -(c_{x2} - c_{x3} + r_2\cos\phi)\sec(2\theta - 2\phi)$$

The analytic expression for the third intersection point (intersection with the vertical screen) is given by:

$$p_{3y}(\theta,\phi) = c_{y2} + r_2\sec(2\theta-2\phi)\sin(2\theta-\phi) + (c_{x2} - c_{x3})\tan(2\theta - 2\phi)$$

By expanding $d_3(\theta,\phi)$ and $p_{3y}(\theta)$ using known trigonometric identities so that only $sin(\phi)$ and $cos(\phi)$ terms are present one can follow up with direct substitution.

## Analytic evaluation of the optical path using the rational parameterization

### Evaluation of $d_1$

We have already seen that the analytic expression of $d_1$ as a function of $\theta$ is :

$$d_1 = (c_{1x} - p_{0x}) - |r_1 cos(\theta)| \tag{6.9}$$

where $p_{0x}$ is the $x$ coordinate of the plane rays start from and $c_{1x}$ is the $x$ coordinate of the centre of the first surface. In order to express the above as a function of $m$ we make the direct substitution

$$cos(\theta) \rightarrow \Big(\frac{m^2 - 1}{m^2 + 1}\Big)$$

So we get :

$$d_1 = (c_{1x} - p_{0x}) - \left| r_1 \Big(\frac{m^2 - 1}{m^2 + 1}\Big) \right| \tag{6.10}$$

**Evaluation of $d_2$**

We have already seen that the expression for $d_2$ as a function of the angular parameter $\theta$ is given by :

$$d_2 = \frac{1}{2}(2r_1\cos(\theta) - 2\cos(2\theta)\delta_x - 2\sin(2\theta)\delta_y)) + \sqrt{-4r_1^2\sin^2(\theta) + 8r_1\sin(\theta)\left(\sin(2\theta)\delta_x - \cos(2\theta)\delta_y\right) + 4r_2^2 - 4\left(\cos(2\theta)\delta_x - \sin(2\theta)\delta_y\right)^2} \tag{6.11}$$

where $\delta_x = c_{2x} - c_{1x},\ \delta_y = c_{2y} - c_{1y}$. Here we can see that terms like $sin(2\theta), cos(2\theta)$ appear. To express these as functions of $m$ we expand using known trigonometric identities:

$$cos(2\theta) = cos^2(\theta) - sin^2(\theta)$$
$$sin(2\theta) = 2cos(\theta)sin(\theta)$$

Using the substitutions :

$$cos(\theta) \to \left(\frac{m^2-1}{m^2+1}\right)$$
$$sin(\theta) \to \left(\frac{-2m}{m^2+1}\right) \tag{6.12}$$

We have

$$cos(2\theta) \to \frac{m^4 - 6m^2 + 1}{(m^2+1)^2}$$
$$sin(2\theta) \to -\frac{4m\left(m^2-1\right)}{(m^2+1)^2}$$

So Eq. (6.11) becomes :

$$\frac{1}{\left(1+m^2\right)^2}\left(\left(1-6\,m^2+m^4\right)c_{x1} - c_{x2} + 4\,m\,c_{y1} - 4\,m\,c_{y2} - r_1 + m^2\left(-\left(-6+m^2\right)c_{x2} + m\left(-4\,c_{y1} + 4\,c_{y2} + m\,r_1\right)\right) + \sqrt{\left(\left(-4\,m\left(-1+m^2\right)\left(c_{x1}-c_{x2}\right) - \left(1-6\,m^2+m^4\right)c_{y1} + \left(1-6\,m^2+m^4\right)c_{y2} - 2\,m\left(1+m^2\right)r_1 + \left(1+m^2\right)^2 r_2\right)\left(4\,m\left(-1+m^2\right)\left(c_{x1}-c_{x2}\right) + \left(1-6\,m^2+m^4\right)c_{y1} - \left(1-6\,m^2+m^4\right)c_{y2} + 2\,m\left(1+m^2\right)r_1 + \left(1+m^2\right)^2 r_2\right)\right)\right)$$

Figure 43: Expression for $d_2(m)$.

### Evaluation of $d_3$

At the first part of the appendix we saw how we may calculate $d_3(\theta)$. Using the methods developed for the calculation of $d_2(m)$ by substituting the trigonometric functions with rational ones, we present the expression for $d_3(m)$. We also perform a coordinate shift so that $\mathbf{c_1} = (0,0), \mathbf{c_2} = L(\cos\omega, \sin\omega)$. In that way the expression is more compact.

$$
\left(2 r_2^2 \left(-2 L \left(1-6 m^2+m^4\right)^2 \text{Cos}[\omega]+8 L m \left(-1+7 m^2-7 m^4+m^6\right) \text{Sin}[\omega]+\right.\right.
$$
$$
2 \left(1+m^2\right)^4 c_{x3}-\left(-1+m^2\right) \left(1+m^2\right)^3 r_1+\left(-1+14 m^2-14 m^6+m^8\right) r_1+
$$
$$
\sqrt{2} \left(1+m^2\right)^2 \left(1-6 m^2+m^4\right) \sqrt{\left(-L^2+\frac{L^2 \left(1-28 m^2+70 m^4-28 m^6+m^8\right) \text{Cos}[2 \omega]}{\left(1+m^2\right)^4}-\right.}
$$
$$
\frac{8 L^2 m \left(-1+7 m^2-7 m^4+m^6\right) \text{Sin}[2 \omega]}{\left(1+m^2\right)^4}+\frac{32 L m^2 \left(-1+m^2\right) \text{Cos}[\omega] r_1}{\left(1+m^2\right)^3}-
$$
$$
\left.\left.\left.\frac{4 L m \text{Sin}[\omega] r_1}{1+m^2}+\frac{4 L m \left(3-10 m^2+3 m^4\right) \text{Sin}[\omega] r_1}{\left(1+m^2\right)^3}-r_1^2+\frac{\left(1-6 m^2+m^4\right) r_1^2}{\left(1+m^2\right)^2}+2 r_2^2\right)\right)\right) \Big/
$$
$$
\left(\left(1+m^2\right)^4 \left(-\frac{2 L^2 \left(1-6 m^2+m^4\right)}{\left(1+m^2\right)^2}-\frac{64 L^2 m^2 \left(-1+m^2\right)^2 \left(1-6 m^2+m^4\right) \text{Cos}[\omega]^2}{\left(1+m^2\right)^6}+\right.\right.
$$
$$
\frac{L^2 \left(1-6 m^2+m^4+\frac{1-66 m^2+495 m^4-924 m^6+495 m^8-66 m^{10}+m^{12}}{\left(1+m^2\right)^4}\right) \text{Cos}[2 \omega]}{\left(1+m^2\right)^2}-\frac{3 L^2 \left(1-6 m^2+m^4\right) \text{Sin}[\omega]^2}{\left(1+m^2\right)^2}-
$$
$$
\frac{L^2 \left(1-66 m^2+495 m^4-924 m^6+495 m^8-66 m^{10}+m^{12}\right) \text{Sin}[\omega]^2}{\left(1+m^2\right)^6}-\frac{4 L^2 m \left(-1+m^2\right) \text{Sin}[2 \omega]}{\left(1+m^2\right)^2}-
$$
$$
\frac{4 L^2 m \left(-3+55 m^2-198 m^4+198 m^6-55 m^8+3 m^{10}\right) \text{Sin}[2 \omega]}{\left(1+m^2\right)^6}+\frac{16 L m \text{Sin}[\omega] r_1}{1+m^2}-
$$
$$
\frac{8 L m \left(3-10 m^2+3 m^4\right) \text{Sin}[\omega] r_1}{\left(1+m^2\right)^3}+\frac{8 L m \left(5-60 m^2+126 m^4-60 m^6+5 m^8\right) \text{Sin}[\omega] r_1}{\left(1+m^2\right)^5}+2 r_1^2-
$$
$$
\frac{4 \left(1-6 m^2+m^4\right) r_1^2}{\left(1+m^2\right)^2}+\frac{2 \left(1-28 m^2+70 m^4-28 m^6+m^8\right) r_1^2}{\left(1+m^2\right)^4}+\frac{4 \left(1-6 m^2+m^4\right) r_2^2}{\left(1+m^2\right)^2}+\frac{1}{\left(1+m^2\right)^4}
$$
$$
16 \sqrt{2} L m \left(-1+7 m^2-7 m^4+m^6\right) \text{Sin}[\omega] \sqrt{\left(-L^2+\frac{L^2 \left(1-28 m^2+70 m^4-28 m^6+m^8\right) \text{Cos}[2 \omega]}{\left(1+m^2\right)^4}-\right.}
$$
$$
\frac{8 L^2 m \left(-1+7 m^2-7 m^4+m^6\right) \text{Sin}[2 \omega]}{\left(1+m^2\right)^4}+\frac{32 L m^2 \left(-1+m^2\right) \text{Cos}[\omega] r_1}{\left(1+m^2\right)^3}-
$$
$$
\left.\frac{4 L m \text{Sin}[\omega] r_1}{1+m^2}+\frac{4 L m \left(3-10 m^2+3 m^4\right) \text{Sin}[\omega] r_1}{\left(1+m^2\right)^3}-r_1^2+\frac{\left(1-6 m^2+m^4\right) r_1^2}{\left(1+m^2\right)^2}+2 r_2^2\right)-
$$
$$
\frac{1}{1+m^2} 2 \sqrt{2} \left(-1+m^2\right) r_1 \sqrt{\left(-L^2+\frac{L^2 \left(1-28 m^2+70 m^4-28 m^6+m^8\right) \text{Cos}[2 \omega]}{\left(1+m^2\right)^4}-\right.}
$$
$$
\frac{8 L^2 m \left(-1+7 m^2-7 m^4+m^6\right) \text{Sin}[2 \omega]}{\left(1+m^2\right)^4}+\frac{32 L m^2 \left(-1+m^2\right) \text{Cos}[\omega] r_1}{\left(1+m^2\right)^3}-\frac{4 L m \text{Sin}[\omega] r_1}{1+m^2}+
$$
$$
\left.\frac{4 L m \left(3-10 m^2+3 m^4\right) \text{Sin}[\omega] r_1}{\left(1+m^2\right)^3}-r_1^2+\frac{\left(1-6 m^2+m^4\right) r_1^2}{\left(1+m^2\right)^2}+2 r_2^2\right)+\frac{1}{\left(1+m^2\right)^3}
$$
$$
2 \sqrt{2} \left(-1+15 m^2-15 m^4+m^6\right) r_1 \sqrt{\left(-L^2+\frac{L^2 \left(1-28 m^2+70 m^4-28 m^6+m^8\right) \text{Cos}[2 \omega]}{\left(1+m^2\right)^4}-\right.}
$$
$$
\frac{8 L^2 m \left(-1+7 m^2-7 m^4+m^6\right) \text{Sin}[2 \omega]}{\left(1+m^2\right)^4}+\frac{32 L m^2 \left(-1+m^2\right) \text{Cos}[\omega] r_1}{\left(1+m^2\right)^3}-\frac{4 L m \text{Sin}[\omega] r_1}{1+m^2}+
$$
$$
\left.\frac{4 L m \left(3-10 m^2+3 m^4\right) \text{Sin}[\omega] r_1}{\left(1+m^2\right)^3}-r_1^2+\frac{\left(1-6 m^2+m^4\right) r_1^2}{\left(1+m^2\right)^2}+2 r_2^2\right)+\frac{1}{\left(1+m^2\right)^6}
$$
$$
32 L m \left(1-m^2\right) \text{Cos}[\omega] \left(L \left(1-6 m^2+m^4\right)^2 \text{Sin}[\omega]+2 m \left(1+m^2\right)^3 r_1-2 m \left(1+m^2\right) \left(3-10 m^2+3 m^4\right) r_1-\right.
$$
$$
2 \sqrt{2} m \left(-1+m^2\right) \left(1+m^2\right)^2 \sqrt{\left(-L^2+\frac{L^2 \left(1-28 m^2+70 m^4-28 m^6+m^8\right) \text{Cos}[2 \omega]}{\left(1+m^2\right)^4}-\right.}
$$
$$
\frac{8 L^2 m \left(-1+7 m^2-7 m^4+m^6\right) \text{Sin}[2 \omega]}{\left(1+m^2\right)^4}+\frac{32 L m^2 \left(-1+m^2\right) \text{Cos}[\omega] r_1}{\left(1+m^2\right)^3}-
$$
$$
\left.\left.\left.\left.\frac{4 L m \text{Sin}[\omega] r_1}{1+m^2}+\frac{4 L m \left(3-10 m^2+3 m^4\right) \text{Sin}[\omega] r_1}{\left(1+m^2\right)^3}-r_1^2+\frac{\left(1-6 m^2+m^4\right) r_1^2}{\left(1+m^2\right)^2}+2 r_2^2\right)\right)\right)\right)
$$

Figure 44: Expression for $d_3(m)$.

# References


[1] URL https://pages.mtu.edu/~shene/COURSES/cs3621/NOTES/curves/rational.html.

[2] M. V. Berry and N. L. Balazs. *Nonspreading wavepackets*. Americal Journal of Physics, 47(3):264–267, 1979.

[3] M. Born and E. Wolf. Principles of Optics: 60th Anniversary Edition. Cambridge University Press, 7 edition, 2019. doi: 10.1017/9781108769914.

[4] Z. Cao, C. Zhai, J. Li, F. Xian, and S. Pei. Light sheet based on one-dimensional airy beam generated by single cylindrical lens. Optics Communications, 393:11–16, 2017.

[5] J. W. Goodman. Introduction to Fourier Optics. McGraw-Hill, New York, 2nd edition, 1996.

[6] E. Hecht. Optics, eBook, Global Edition. Pearson Education, 2016. ISBN 9781292096964. URL https://books.google.gr/books?id=kv4yDQAAQBAJ.

[7] D. Mansour and D. G. Papazoglou. Ultra-broadband tunable continuous phase masks using optical aberrations. Optics Letters, 43(21):5480–5483, 2018.

[8] D. Papazoglou, S. Suntsov, D. Abdollahpour, and S. Tzortzakis. Tunable intense airy beams and tailored femtosecond laser filaments. Physical Review A, 81(6):061807, 2010.

[9] D. G. Papazoglou. Lecture notes on Foundations of Modern Optics, 2013.

[10] J. Rayces. Exact relation between wave aberration and ray aberration. Optica Acta: International Journal of Optics, 11(2):85–88, 1964.

[11] G. A. Siviloglou and D. N. Christodoulides. *Accelerating finite energy Airy beams*. Optics Letters, 32(8):979, 2007.

[12] O. Vallée and M. Soares. Airy Functions and Applications to Physics. IMPERIAL COLLEGE PRESS, sep 2004. ISBN 978-1-86094-478-9. doi: 10.1142/p345. URL http://www.worldscientific.com/worldscibooks/10.1142/p345.

[13] ZEMAX Optical Design Program, ZEMAX Development Corporation, USA.